geodiversitas

2023 • 45 • 22

A new platyrostrine sperm whale from the Early Miocene of the southeastern Pacific (East Pisco Basin, Peru) supports affinities with the southwestern Atlantic cetacean fauna

Olivier LAMBERT, Alberto COLLARETA, Aldo BENITES-PALOMINO, Marco MERELLA, Christian de MUIZON, Rebecca BENNION, Mario URBINA & Giovanni BIANUCCI

art. 45 (22) — Published on 30 November 2023
www.geodiversitas.com

PUBLICATIONS SCIENTIFIQUES

MUSÉUM NAL HIST NATURELLE

Geodiversitas est indexé dans / Geodiversitas *is indexed in:*
– Science Citation Index Expanded (SciSearch®)
– ISI Alerting Services®
– Current Contents® / Physical, Chemical, and Earth Sciences®
– Scopus®

Geodiversitas est distribué en version électronique par / Geodiversitas *is distributed electronically by:*
– BioOne® (http://www.bioone.org)

Les articles ainsi que les nouveautés nomenclaturales publiés dans *Geodiversitas* sont référencés par / *Articles and nomenclatural novelties published in* Geodiversitas *are referenced by:*
– ZooBank® (http://zoobank.org)

Geodiversitas est une revue en flux continu publiée par les Publications scientifiques du Muséum, Paris
Geodiversitas *is a fast track journal published by the Museum Science Press, Paris*

Les Publications scientifiques du Muséum publient aussi / *The Museum Science Press also publish:* ***Adansonia***, ***Zoosystema***, ***Anthropozoologica***, ***European Journal of Taxonomy***, ***Naturae***, ***Cryptogamie*** **sous-sections** ***Algologie***, ***Bryologie***, ***Mycologie, Comptes Rendus Palevol***

Diffusion – Publications scientifiques Muséum national d'Histoire naturelle
CP 41 – 57 rue Cuvier F-75231 Paris cedex 05 (France)
Tél. : 33 (0)1 40 79 48 05 / Fax : 33 (0)1 40 79 38 40
diff.pub@mnhn.fr / http://sciencepress.mnhn.fr

ISSN (imprimé / *print*) : 1280-9659/ ISSN (électronique / *electronic*) : 1638-9395

A new platyrostrine sperm whale from the Early Miocene of the southeastern Pacific (East Pisco Basin, Peru) supports affinities with the southwestern Atlantic cetacean fauna

Olivier LAMBERT
D.O. Terre et Histoire de la Vie, Institut royal des Sciences naturelles de Belgique,
29 rue Vautier, B-1000 Brussels (Belgium)
olivier.lambert@naturalsciences.be (corresponding author)

Alberto COLLARETA
Dipartimento di Scienze della Terra, Università di Pisa, via S. Maria 53, I-56126 Pisa (Italy)
and Museo di Storia Naturale, Università di Pisa, via Roma 79, I-56011 Calci (Italy)
alberto.collareta@unipi.it

Aldo BENITES-PALOMINO
Department of Paleontology, University of Zürich,
Karl-Schmid-Strasse 4, CH-8006 Zürich (Switzerland)
and Departamento de Paleontología de Vertebrados, Museo de Historia Natural-Universidad Nacional
Mayor de San Marcos, Avenida Arenales 1256, P-15072 Lima 11 (Peru)
aldo.benitespalomino@uzh.ch

Marco MERELLA
Dipartimento di Scienze della Terra, Università di Pisa, via S. Maria 53, I-56126 Pisa (Italy)
and Dottorato Regionale in Scienze della Terra "Pegaso", via S. Maria 53, I-56126 Pisa (Italy)
marco.merella@phd.unipi.it

Christian de MUIZON
CR2P (CNRS, MNHN, Sorbonne Université), Département Origines et Évolution,
Muséum national d'Histoire naturelle, case postale 38, 57 rue Cuvier, F-75231 Paris cedex 05 (France)
muizon@mnhn.fr

Rebecca BENNION
D.O. Terre et Histoire de la Vie, Institut royal des Sciences naturelles de Belgique,
29 rue Vautier, B-1000 Brussels (Belgium)
and Evolution & Diversity Dynamics Lab, UR Geology, Université de Liège,
14 Allée du 6 Août, B-4000 Liège (Belgium)
r.bennion@uliege.be

Mario URBINA
Departamento de Paleontología de Vertebrados, Museo de Historia Natural-Universidad Nacional
Mayor de San Marcos, Avenida Arenales 1256, P-15072 Lima (Peru)
mariourbina01@hotmail.com

Giovanni BIANUCCI
Dipartimento di Scienze della Terra, Università di Pisa, via S. Maria 53, I-56126 Pisa (Italy)
and Museo di Storia Naturale, Università di Pisa, via Roma 79, I-56011 Calci (Italy)
giovanni.bianucci@unipi.it

Submitted on 5 April 2023 | accepted on 18 July 2023 | published on 30 November 2023

urn:lsid:zoobank.org:pub:74B9ACDB-AEF0-40C4-97C8-D12D071A4CD4

Lambert O., Collareta A., Benites-Palomino A., Merella M., Muizon C. de, Bennion R., Urbina M. & Bianucci G. 2023. — A new platyrostrine sperm whale from the Early Miocene of the southeastern Pacific (East Pisco Basin, Peru) supports affinities with the southwestern Atlantic cetacean fauna. *Geodiversitas* 45 (22): 659-679. https://doi.org/10.5252/geodiversitas2023v45a22. http://geodiversitas.com/45/22

ABSTRACT

Contrasting with their suction feeding modern relatives in the families Kogiidae and Physeteridae, Miocene physeteroids display a broad range of feeding strategies. Despite the continuous improvements of the fossil record, the transition from the earliest sperm whales to suction feeding forms as well as the once prominent macroraptorial forms remains poorly understood. In the present work, we investigate a partial sperm whale skull from Lower Miocene (Burdigalian) strata of the Chilcatay Formation of the East Pisco Basin, along the southern coast of Peru. Based on this specimen, we describe a new species in the genus *Diaphorocetus* Ameghino, 1894, which was previously known only by the holotype of *Diaphorocetus poucheti* (Moreno, 1892) from a roughly synchronous unit in Patagonia (Argentina). Differing from the latter in its smaller cranial dimensions, higher tooth count, and minor differences in the position of facial foramina, the new species *Diaphorocetus ortegai* n. sp. confirms a key character of *D. poucheti*, the marked dorsoventral flattening of the maxillary portion of the rostrum. Such cranial proportions suggest that, compared to other physeteroids, *D. poucheti* and *D. ortegai* n. sp. were more efficient at performing fast lateral sweeps of their rostra to capture small- to medium-sized prey items with their proportionally small teeth. Recovered as stem physeteroids in our phylogenetic analysis, these sister species contribute to the ecomorphological disparity of sperm whales during the Early Miocene, but without displaying any of the cranial and dental changes occurring in later, macroraptorial and suction feeding sperm whales. The description of a new species of *Diaphorocetus* from southern Peru increases the similarities between the toothed whale faunas from the local Chilcatay Formation and the Gaiman and Monte Leon formations of Argentinian Patagonia, pointing not only to dispersal routes between the southeastern Pacific and southwestern Atlantic during the Burdigalian, but also to relatively similar ecological settings along the coasts of Peru and Patagonia at that time.

KEY WORDS
Physeteroidea,
Burdigalian,
Chilcatay Formation,
Diaphorocetus,
feeding,
dispersal,
Argentina,
new species.

RÉSUMÉ

Un nouveau cachalot platyrostre du Miocène inférieur du Pacifique sud-est (est du bassin de Pisco, Pérou) consolide les affinités avec la faune de cétacés de l'Atlantique sud-ouest.

À la différence de leurs parents modernes dans les familles Kogiidae et Physeteridae, qui se nourrissent en aspirant leurs proies, les physétéroïdés miocènes présentent un large éventail de stratégies d'alimentation. Malgré les améliorations continues du registre fossile, la transition des premiers cachalots aux formes se nourrissant par aspiration ainsi qu'aux formes macroraptoriales, autrefois importantes, reste mal comprise. Dans ce travail, nous étudions un crâne partiel de cachalot des couches du Miocène inférieur (Burdigalien) de la Formation Chilcatay, à l'est du bassin de Pisco, le long de la côte sud du Pérou. Sur base de ce spécimen, nous décrivons une nouvelle espèce dans le genre *Diaphorocetus* Ameghino, 1894, qui n'était auparavant connu que par l'holotype de *Diaphorocetus poucheti* (Moreno, 1892) provenant d'une unité approximativement synchrone en Patagonie (Argentine). Différant de cette dernière espèce par ses dimensions crâniennes plus petites, son nombre de dents plus élevé, et des différences mineures dans la position des foramens faciaux, la nouvelle espèce *Diaphorocetus ortegai* n. sp. confirme un caractère-clé de *D. poucheti*, l'aplatissement dorso-ventral marqué de la partie maxillaire du rostre. De telles proportions crâniennes suggèrent que, par rapport aux autres physétéroïdés, *D. poucheti* et *D. ortegai* n. sp. étaient plus efficaces pour effectuer des balayages latéraux rapides avec leur rostre, afin de capturer des proies de taille petite à moyenne avec leurs dents proportionnellement petites. Identifiées en tant que physétéroïdés souches dans notre analyse phylogénétique, ces espèces sœurs contribuent à la disparité écomorphologique des cachalots au début du Miocène, mais sans présenter aucun des changements crâniens et dentaires survenant chez les cachalots macroraptoriaux ou aspirant leurs proies. La description d'une nouvelle espèce de *Diaphorocetus* sur la côte sud du Pérou augmente les similitudes notées entre les faunes de cétacés à dents de la Formation Chilcatay locale et les formations Gaiman et Monte Leon de Patagonie, indiquant non seulement des voies de dispersion entre le sud-est du Pacifique et le sud-ouest de l'Atlantique au cours du Burdigalien, mais aussi des conditions écologiques relativement similaires le long des côtes du Pérou et de Patagonie à cette époque.

MOTS CLÉS
Physeteroidea,
Burdigalien,
Formation Chilcatay,
Diaphorocetus,
nutrition,
dispersion,
Argentine,
espèce nouvelle.

INTRODUCTION

The Early Miocene represents a key time interval for the evolutionary history of cetaceans, witnessing the extinction (or strong decline) of several Oligocene clades of toothed mysticetes and heterodont odontocetes, along with the earliest radiations of modern groups – including balaenids, platanistoids, delphinidans, and physeteroids – prior to the Mid-Miocene Climatic Optimum (Steeman *et al.* 2009; Marx *et al.* 2016; Buono *et al.* 2017; Marx *et al.* 2019). With respect to physeteroids (sperm

whales), the extant members of the families Kogiidae and Physeteridae are known as highly specialized suction-feeders (Werth 2004; Bloodworth & Marshall 2005) that mostly forage on mesopelagic prey, thus playing a major ecological role in the transfer of nutrients from the oceanic depths to the photic zone along with other deep-diving cetaceans (Lavery *et al.* 2010). Though some progress has been recently done concerning the palaeobiology of kogiids (e.g., Velez-Juarbe *et al.* 2015; Benites-Palomino *et al.* 2020, 2021; Collareta *et al.* 2017, 2020) and macroraptorial sperm whales (Lambert & Bianucci 2019; Peri *et al.* 2022a), the mode and tempo of the transition from a raptorial to a suction-assisted feeding strategy (Hocking *et al.* 2017) in extinct physeteroids remain poorly understood. This is due to various factors, including: i) the relatively low number of Neogene species known from well-preserved cranial and dental material, which makes it difficult to discuss feeding techniques in depth (e.g., Kimura & Hasegawa 2022; Peri *et al.* 2022b); ii) the low resolution and support of physeteroid phylogenetic trees, and especially the lack of consensus and ambiguity about the stem physeteroid-physeterid transition (e.g., Paolucci *et al.* 2020; Alfsen *et al.* 2021; Peri *et al.* 2022b); and iii) the poorly constrained stratigraphic range of several species (e.g., Lambert 2008; Paolucci *et al.* 2020). To further investigate the early evolutionary steps of sperm whales, both coasts of South America are areas with good potential, as they have already yielded well-preserved physeteroid material dating back to the Burdigalian (late Early Miocene) (Lydekker 1893; Bianucci *et al.* 2018b; Lambert *et al.* 2020; Paolucci *et al.* 2020). In the present paper, we describe and compare a physeteroid cranium from the Burdigalian of the Chilcatay Formation, East Pisco Basin, southern coast of Peru. This cranium was previously mentioned in the faunal list of the temporally well-constrained locality of Ullujaya (Bianucci *et al.* 2018b), but without providing any description. We investigate its phylogenetic relationships, comment on its feeding strategy, and discuss the odontocete faunal similarities between the southeastern Pacific and southwestern Atlantic during the Burdigalian.

MATERIAL AND METHODS

Abbreviations

Institutional abbreviations

MLP	Museo de La Plata, La Plata, Argentina;
MUSM	Museo de Historia Natural, Universidad Nacional Mayor de San Marcos, Lima, Peru.

Anatomical abbreviations

BZW	bizygomatic width;
CBL	condylobasal length.

Anatomical terminology

For the anatomy of the skull, we primarily follow Mead & Fordyce (2009), with a few exceptions for morphological features that are specific to physeteroids, for which we refer to Flower (1867), Kellogg (1927, 1965), and Bianucci & Landini (2006).

Surface scanning

Textured 3D models of the skulls of MUSM 3246, MUSM 2543 (holotype of *Rhaphicetus valenciae* Lambert, Muizon, Urbina & Bianucci, 2020), and MUSM 1399 (holotype of *Acrophyseter robustus* Lambert, Bianucci & Muizon, 2016, including the rediscovered tip of the snout) were obtained with an Artec Eva structured-light scanner for MUSM 3246 and SHINING EinScan Pro HD structured-light scanner for the two other skulls (see Appendices 1-3). The two parts of the cranium of MUSM 2543 (anterior two thirds of rostrum and rest of the cranium) and skull of MUSM 1399 (tip of snout and rest of the skull) were assembled with Blender 3.0.1.

Phylogenetic analyses

To investigate the phylogenetic relationships of the new specimen, we scored it in the morphological character-taxon matrix of Peri *et al.* (2022b), which in turn derives from those of Alfsen *et al.* (2021) and Lambert *et al.* (2017). The formulation of one character (char. 13) was slightly modified; four new characters (char. 55-58) were added, resulting in a matrix of 58 characters, scored for 35 taxa, including three outgroups (the basilosaurids *Cynthiacetus peruvianus* (Martínez-Cáceres & Muizon, 2011) and *Zygorhiza kochi* (Reichenbach, 1847), and the stem odontocete *Agorophius pygmaeus* (Müller, 1849) and 32 physeteroids (see Appendix 1 for the list of characters and Appendix 4 for the character-taxon matrix). Two scores were modified for *Diaphorocetus poucheti* based on the reinterpretation of the type specimen (char. 28: 1 => 0; char. 44: 1 => 0) and new scores were added for the holotype of *Acrophyseter robustus*, due to the recovery of the lost tip of the rostrum in the MUSM collection, providing information about rostrum length, anterior extent of maxilla and premaxilla, and minimum tooth count (char. 1 => 0; char. 2 => 0; char. 7 => 0; char. 38 => 2; see Appendix 3, for 3D model). As in a recent work that exploited this matrix (Peri *et al.* 2022b), the cladistic analysis was performed with PAUP* 4.0.a169 (Swofford 2003), using the tree-bisection-reconnection algorithm and the heuristic search option; all characters were considered as unordered and unweighted. The resulting strict consensus tree was time-calibrated based on the chronostratigraphic ranges of the analysed taxa as reported by Peri *et al.* (2022b), modified from Paolucci *et al.* (2020: appendix 4) with the addition of ranges for *Rhaphicetus valenciae* and *Thalassocetus* sp. IRSNB M.2329 following Lambert *et al.* (2020) and Alfsen *et al.* (2021), respectively, with adjustments for *Acrophyseter* spp., *Cozzuoliphyseter rionegrensis* (Gondar, 1975), *Diaphorocetus poucheti*, and *Livyatan melvillei* (Lambert, Bianucci, Post, Muizon, Salas-Gismondi, Urbina & Reumer, 2010) based on a review of the relevant geological literature (Reichler 2010; Bosio *et al.* 2021; Parras & Cuitiño 2021; Cuitiño *et al.* 2023) . Bootstrap values were calculated from 100 tree replicates. Additionally, a cladistic analysis was performed with down-weighting of homoplastic characters (k = 3), as a supplementary test of the phylogenetic relationships of the new specimen.

STRATIGRAPHIC SETTING AND PALAEOENVIRONMENTAL FRAMEWORK

The Chilcatay Formation comprises the Lower Miocene portion of the sedimentary fill of the East Pisco Basin (Fig. 1C), an Andean forearc basin stretching along the southern coast of Peru, whose most representative outcrops are to be found in the coastal desert of the present-day Ica Region (Fig. 1A). Along the western side of the Ica River, including the thoroughly investigated Ullujaya area (Fig. 1B), the Chilcatay strata have been shown to consist of two distinct sequences or allomembers, namely, Ct1 and Ct2 (in ascending stratigraphic order), plus an older sequence (Ct0) that has recently been identified at the remote Media Luna locality, in the southern portion of the basin (DeVries & Jud 2018; Di Celma *et al.* 2018, 2019; DeVries *et al.* 2021; Bosio *et al.* 2022). During the deposition of the Chilcatay strata, the East Pisco Basin was shaped as a shelfal embayment whose seaward border was marked by an archipelago of basement islands (Bianucci *et al.* 2018b; DeVries & Jud 2018).

At Ullujaya, which represents the type locality of the new cetacean species described herein, both Ct1 and Ct2 are exposed. Ct1, in particular, consists of two facies associations, i.e., *Ct1a* (formed by sandstones and siltstones interbedded with conglomerate beds) and *Ct1b* (formed by coarse-grained, largely bioclastic clinostrata). Vertebrate fossils occur abundantly in the *Ct1a* strata (Bianucci *et al.* 2018b; Di Celma *et al.* 2018), which witness to an offshore, shelfal depositional setting (Di Celma *et al.* 2018) below 30-40 m water depth (Coletti *et al.* 2018).

The physeteroid specimen studied herein was identified in the geological map of Ullujaya provided by Di Celma *et al.* (2018) with the field number O1. It originates from a silty sand horizon located 25.9 m above the base of the local section, in the upper part of the *Ct1a* stratal package (see Bianucci *et al.* 2018b; Di Celma *et al.* 2018) (Fig. 1D). This part of the Ct1 allomember has been dated to the late Early Miocene (Burdigalian, between *c.* 19 and 18 Ma, and probably close to 18.4 Ma) based on biostratigraphic data (*Craspedodiscus elegans* diatom zone and the upper part of the *Naviculopsis ponticula* silicoflagellate zone) (Di Celma *et al.* 2018). Radiometric dating of two volcanic ash layers and the application of Strontium Isotope Stratigraphy to selected shell-rich beds (Bosio *et al.* 2020, 2022) allow the age of the studied cetacean specimen to be constrained to the 18.8-18.3 Ma interval (Fig. 1D). The associated toothed whale fauna includes the longirostrine homodont odontocete *Chilcacetus cavirhinus* Lambert, Muizon & Bianucci, 2015 (Lambert *et al.* 2015), the squalodelphinids *Huaridelphis raimondii* Lambert, Bianucci & Urbina, 2014 (Lambert *et al.* 2014) and *Notocetus vanbenedeni* Moreno, 1892 (but see Viglino *et al.* 2022 for a different taxonomic assessment of the Peruvian specimens referred by Bianucci *et al.* 2015 to the latter taxon), and the kentriodontid *Kentriodon* sp. (Bianucci *et al.* 2018b). Fish remains, mostly consisting of shark and ray teeth and spines, are also abundant in the same strata; they depict a coastal palaeocommunity, as well as a warm-temperate, sheltered palaeoenvironment connected with both riverine and open-sea habitats (Bianucci *et al.* 2018b). The archaic leatherback turtle *Natemys peruvianus* Wood, Johnson-Gove, Gaffney & Maley, 1996 also likely originates from the Chilcatay strata cropping out at Ullujaya, but its precise stratigraphic whereabouts are unknown (Bianucci *et al.* 2018b).

Other localities where the Burdigalian portion of the Chilcatay Formation is exposed have so far yielded further forms of cetaceans (Bianucci *et al.* 2018a, 2020; Lambert *et al.* 2018, 2020, 2021; Di Celma *et al.* 2019), elasmobranchs (Shimada *et al.* 2017; Di Celma *et al.* 2019; Landini *et al.* 2019; Collareta *et al.* 2022, 2023), sea birds (Acosta-Hospitaleche & Stucchi 2005), and bony fishes (Di Celma *et al.* 2019). In particular, another physeteroid species, *Rhaphicetus valenciae*, has recently been described from the highly fossiliferous locality of Zamaca, and specifically from deposits belonging the *Ct1a* stratal package (Lambert *et al.* 2020) (Fig. 1E).

SYSTEMATIC PALAEONTOLOGY

Order CETACEA Brisson, 1762
Clade PELAGICETI Uhen, 2008
Clade NEOCETI Fordyce & Muizon, 2001
Suborder ODONTOCETI Flower, 1867b
Superfamily PHYSETEROIDEA Gray, 1821
stem PHYSETEROIDEA

Genus *Diaphorocetus* Ameghino, 1894

TYPE SPECIES. — *Mesocetus poucheti* Moreno, 1892, by monotypy, known from a single specimen thought to originate from Burdigalian deposits of the Gaiman Formation, in the Chubut province, Argentina (see Paolucci *et al.* 2020 for the complex taxonomic history of this species).

OTHER REFERRED SPECIES. — *Diaphorocetus ortegai* n. sp.

REMARKS

The referral of a new species to the genus *Diaphorocetus* allows for the addition of one synapomorphy to the detailed emended diagnosis provided by Paolucci *et al.* (2020): dorsoventral flattening of the maxilla on the rostrum (ratio between maximum dorsoventral height of maxilla along the anterior half of the rostrum and bizygomatic width < 0.1, only shared with *Acrophyseter deinodon* Lambert, Bianucci & Muizon, 2008 and *Zygophyseter varolai* Bianucci & Landini, 2006). Whereas most differential characters provided by Paolucci *et al.* (2020) apply to the new species, we propose to remove the following characters from the genus diagnosis: i) 'rostrum [...] contributing 50% of CBL', as the rostrum is incomplete on the types of both the included species; ii) 'zygomatic process of squamosal with ventrally deflected apex', as we interpret this condition as at least partly resulting from an inaccurate reconstruction of the type neurocranium of *D. poucheti* (see below); and iii) the differential character 'more open jugular notch', which appears to vary within the genus and could be easily impacted by postmortem deformation and/or reconstruction inaccuracies.

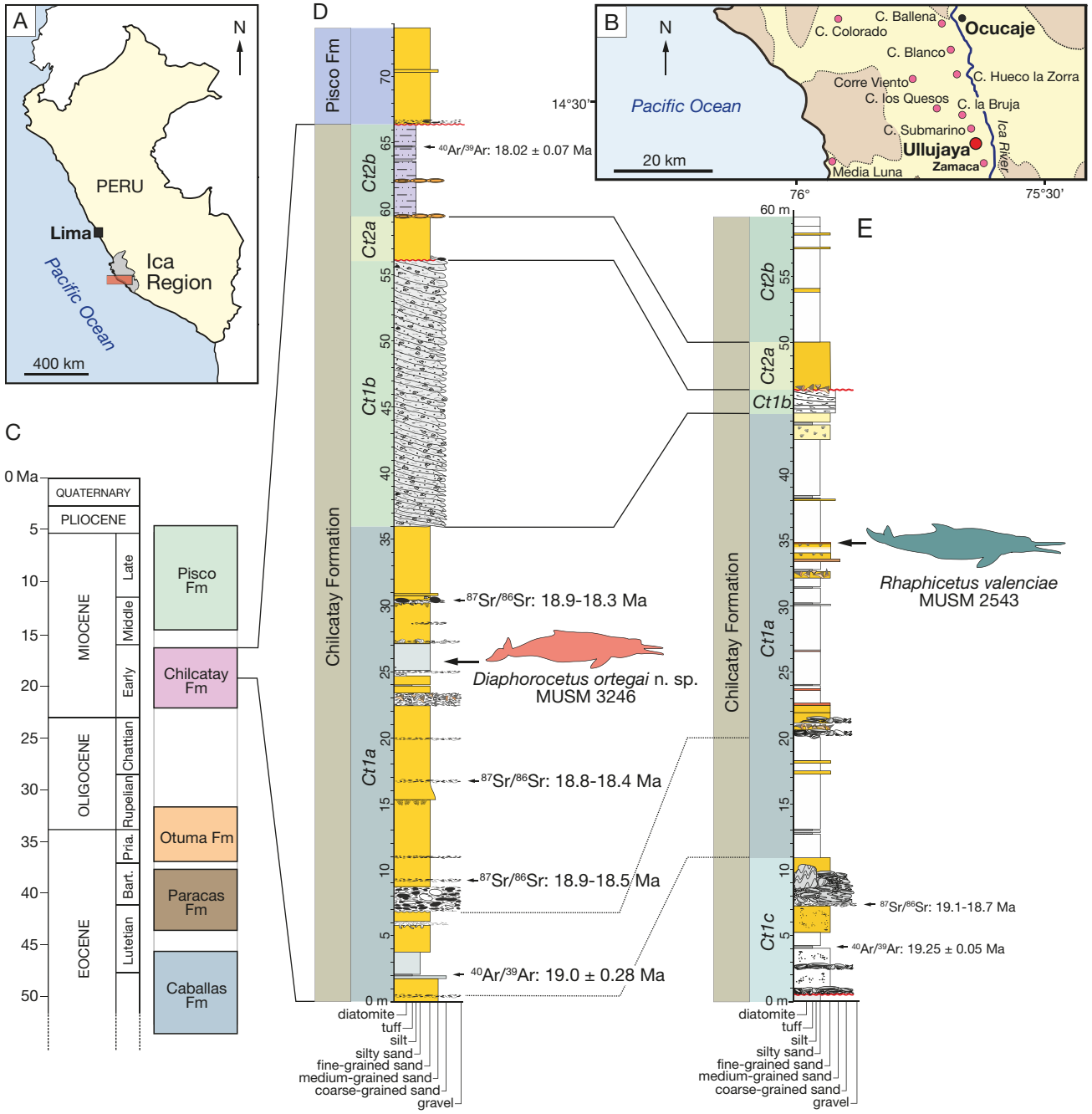

FIG. 1. — Geographic and geological setting. **A**, Location of the main outcrops of the Chilcatay Formation along the southern coast of Peru. **B**, Simplified map providing the position of Ullujaya (the type locality of *Diaphorocetus ortegai* n. sp.) alongside other highly fossiliferous sites of the Ica desert (including Zamaca, the type locality of *Rhaphicetus valenciae* Lambert, Muizon, Urbina & Bianucci, 2020). **C**, Schematic stratigraphic column of the Cenozoic succession exposed in the East Pisco Basin. **D**, Simplified stratigraphic section of the Chilcatay Formation in Ullujaya, showing the exact position of the holotype of *D. ortegai* n. sp. in the Ct1 allomember, *Ct1a* facies association. **E**, Simplified stratigraphic section of the Chilcatay Formation in Zamaca, showing the exact position of the holotype of *R. valenciae* in the Ct1 allomember, *Ct1a* facies association. Both sections **D** and **E** include positions of ash layers dated with $^{40}Ar/^{39}Ar$ and shell-rich beds dated with $^{87}Sr/^{86}Sr$ along with the corresponding age estimates (after Bosio *et al.* 2022). Maps and sections modified from Bianucci *et al.* (2018b), Di Celma *et al.* (2018, 2019), Bosio *et al.* (2020, 2022), and Lambert *et al.* (2020).

Diaphorocetus ortegai n. sp.
(Figs 2-6)

urn:lsid:zoobank.org:act:49F43A5D-ECEB-4D12-AC7A-67FE04881EF4

Physeteroidea indet. – Di Celma *et al.* 2018: main map (supplemental material file #3).

cf. *Diaphorocetus* sp. – Bianucci *et al.* 2018b: 262.

cf. *Diaphorocetus* sp. – Bianucci & Collareta 2022: 36.

DIAGNOSIS. — *Diaphorocetus ortegai* n. sp. is a small- to medium-sized physeteroid (BZW *c.* 500 mm) differing from *Diaphorocetus poucheti* by the following cranial characters: smaller cranial dimensions; higher number of alveoli per length unit along the alveolar

TABLE 1. — Cranial measurements (in mm) of *Diaphorocetus ortegai* n. sp. MUSM 3246 (holotype, Chilcatay Formation, East Pisco Basin, Peru), compared to the type of *Diaphorocetus poucheti* (Moreno, 1892) MLP 5-6 (Gaiman Formation, Puerto Madryn, Chubut, Argentina). Part of the measurements for MLP 5-6 are taken from Paolucci *et al.* (2020); others were taken based on photos. Abbreviations: **+**, incomplete; **e**, estimate; **–**, no data.

	***D. ortegai* n. sp.** **MUSM 3246 (holotype)**	***D. poucheti*** **MLP 5-6 (holotype)**
Condylobasal length	+764	+820
Rostrum length	+434	+491.9
Neurocranium length	330 (e)	+325.8
Width of rostrum along anterior cross section	72	–
Width of rostrum 250 mm anterior to antorbital notch	91	180 (e)
Height of maxilla 250 mm anterior to antorbital notch	e32	40 (e)
Width of rostrum at base	290 (e)	+388
Maximum width of ventral exposure of vomer on rostrum	28	44.1
Transverse width of right bony naris	18	–
Transverse width of left bony naris	39 (e)	–
Maximum posterior width of supracranial basin	235 (e)	278.8
Minimum distance between temporal fossae across occipital shield	202 (e)	225.3
Mediolateral width of left temporal fossa	+120	–
Bizygomatic width	+470	522.9
Distance between ventromedial margins of paroccipital processes	253	350 (e)
Width of occipital condyles	+128	137.2
Number of preserved maxillary alveoli on left side	18/336 mm = 5.4/100 mm	6/143 mm (e) = 4.2/100 mm
Number of preserved maxillary alveoli on right side	18/347 mm = 5.2/100 mm	7/190 mm (e) = 3.7/100 mm
Range of transverse diameters for maxillary alveoli	13-18	–
Range of lengths for interalveolar septa	2.5-11	7-11
Length of upper alveolar groove	+347	+287.2

groove (5.2-5.4/100 mm), most likely resulting in a higher tooth count (>18 per upper toothrow); right premaxillary foramen located posterior to the level of the antorbital notch; and absence of a large dorsal infraorbital foramen in the posterodorsal region of the right maxilla, nearly in line with the nuchal crest.

HOLOTYPE. — MUSM 3246, a partly complete cranium lacking the distal tip of the rostrum, lateral portions of the neurocranium (including most of the supraorbital processes and part of the zygomatic processes of the squamosals), most of the occipital shield, teeth, and ear bones (Figs 2-6; Appendix 2 for 3D model).

TYPE LOCALITY. — Ullujaya, East Pisco Basin, southern coast of Peru. Geographic coordinates: 14°35'06.02"S, 75°38'06.6"W (Fig. 1B).

TYPE HORIZON AND AGE. — Chilcatay Formation, Ct1 allomember, *Ct1a* facies association. The age of the type horizon is constrained to the 18.8-18.3 Ma interval (see above for more details; Fig. 1D).

ETYMOLOGY. — The eponymous name honours Prof. Dr. Hernán Ortega, Peruvian ichthyologist and former director of the Museo de Historia Natural, Universidad Nacional Mayor de San Marcos, for his continuous support of palaeontology in Peru, especially during the early years of the Departamento de Paleontología de Vertebrados at the Museo de Historia Natural.

DESCRIPTION

General cranial morphology

In addition to missing the anterior tip of the rostrum, lateral and posterodorsal portions of the neurocranium, MUSM 3246 is characterized by damaged surfaces, with many post-mortem fractures, especially on the dorsal surface of the rostrum and walls of the supracranial basin, as well as the zygomatic arches. The dorsal surface of the anterior part of the rostrum has been heavily abraded, due to prolonged exposure to weathering in the present-day desert environment. In addition to the truncation of the rostrum, part of the premaxillae has been lost medially along the dorsal portion. Bone surfaces are better preserved ventrally, but a thin layer of sediment has been retained in several places, e.g. in the right orbital region and posterolateral parts of the palate, due to low visual contrast with the underlying spongy bones.

Considering the closed (but not fused) sutures for all the preserved cranial bones, their general robustness, the well-defined mandibular dental alveoli, and the presence of embrasure pits along the palatal surface of the right maxilla (see below), the ontogenetic stage of the individual represented by this cranium is interpreted as adult or subadult. With an estimated BZW of 500 mm, this medium-sized physeteroid was close in cranial width to specimens referred to *Rhaphicetus valenciae* (BZW = 505 mm in holotype), *Placoziphius duboisi* Van Beneden, 1869 (BZW roughly estimated at 490 mm in holotype), and *Orycterocetus crocodilinus* Cope, 1867 (BZW = 485 mm in USNM 22926). Using the BZW equation of Pyenson & Sponberg (2011) for stem physeteroids, body length of MUSM 3246 is estimated to 4.54 m. Most cranial dimensions are smaller than in the holotype of *Diaphorocetus poucheti* (Table 1; Paolucci *et al.* 2020) and, to an even greater extent, *Cozzuoliphyseter rionegrensis* (Paolucci *et al.* 2021). Since the rostrum is truncated at a level where its lateral margins are parallel and distant from each other (Figs 2; 3), it was markedly longer than the neurocranium. The proximal portion of the rostrum is much wider than high in cross section (defined as the platyrostrine condition). In lateral view, the ventral outline of the rostrum is moderately convex in its anterior preserved portion, which is slightly anterodorsally recurved (Fig. 4); it becomes distinctly concave in its most proximal region, thus drawing a typical sigmoid shape.

With the nuchal crest being rectilinear in dorsal view, the supracranial basin has a sub-rectangular posterior outline, as

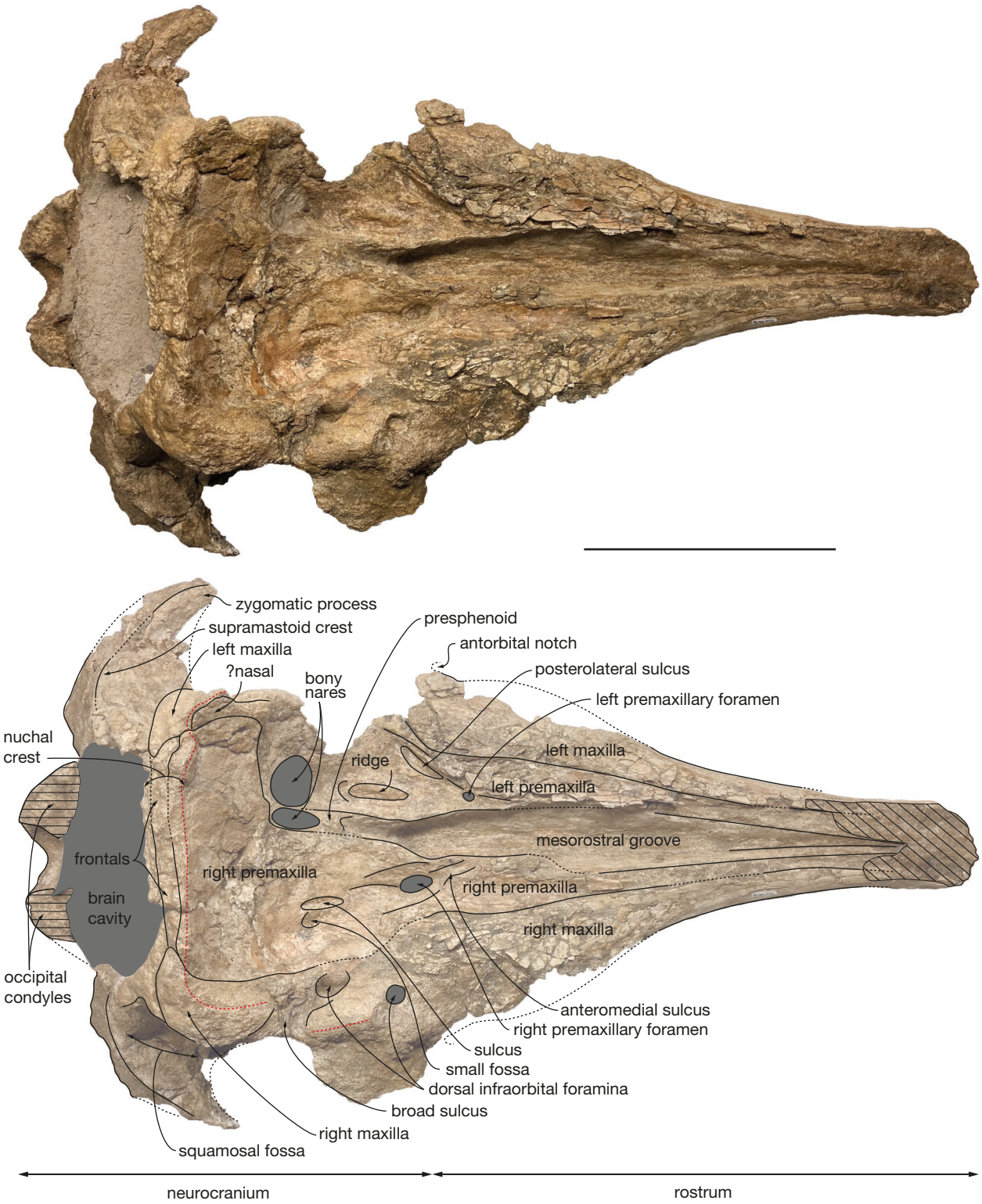

FIG. 2. — Cranium of *Diaphorocetus ortegai* n. sp. MUSM 3246 (holotype, Chilcatay Formation, East Pisco Basin, Peru) in dorsal view; photo and corresponding line drawing. Grey shading for sediment; hatching for main break surfaces; black dashed lines for more tentative interpretations of sutures and edges; and red dashed lines for posterior and lateral outlines of supracranial basin. Scale bar: 200 mm.

seen in *Aulophyseter morricei* Kellogg, 1927, *C. rionegrensis*, *D. poucheti*, and, to a lesser extent, *R. valenciae* (where it is more rounded on the left side). The basin ends posteriorly before the level of the squamosal fossa, and laterally before the level of the antorbital notch (outline of posteromedial margin of left antorbital notch partly preserved in lateral view) (Figs 2; 5; 6). The posterior wall of the basin is low, with the nuchal crest reaching barely higher dorsally than

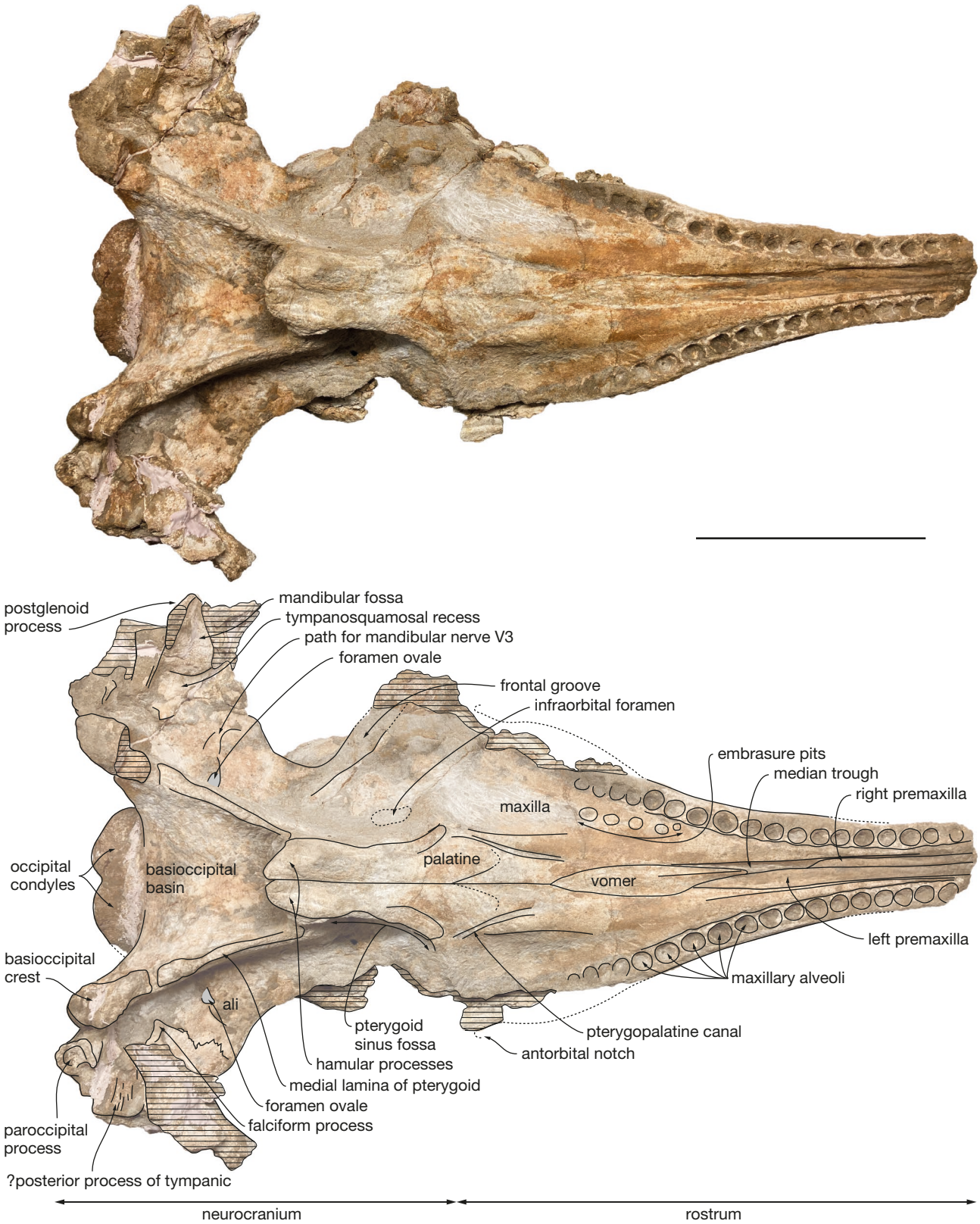

FIG. 3. — Cranium of *Diaphorocetus ortegai* n. sp. MUSM 3246 (holotype, Chilcatay Formation, East Pisco Basin, Peru) in ventral view; photo and corresponding line drawing. Hatching for main break surfaces; black dashed lines for more tentative interpretations of sutures and edges. ali: alisphenoid. Scale bar: 200 mm.

the temporal fossa, 75 mm above the dorsal margin of the right bony naris. This corresponds to a basin that is much less dorsally extended than in e.g. *Acrophyseter* spp., *Orycterocetus crocodilinus*, and *Physeter macrocephalus* Linnaeus, 1758. The dorsomedial elevation of the medial margin of the left premaxilla just anterior to the left premaxillary foramen sug-

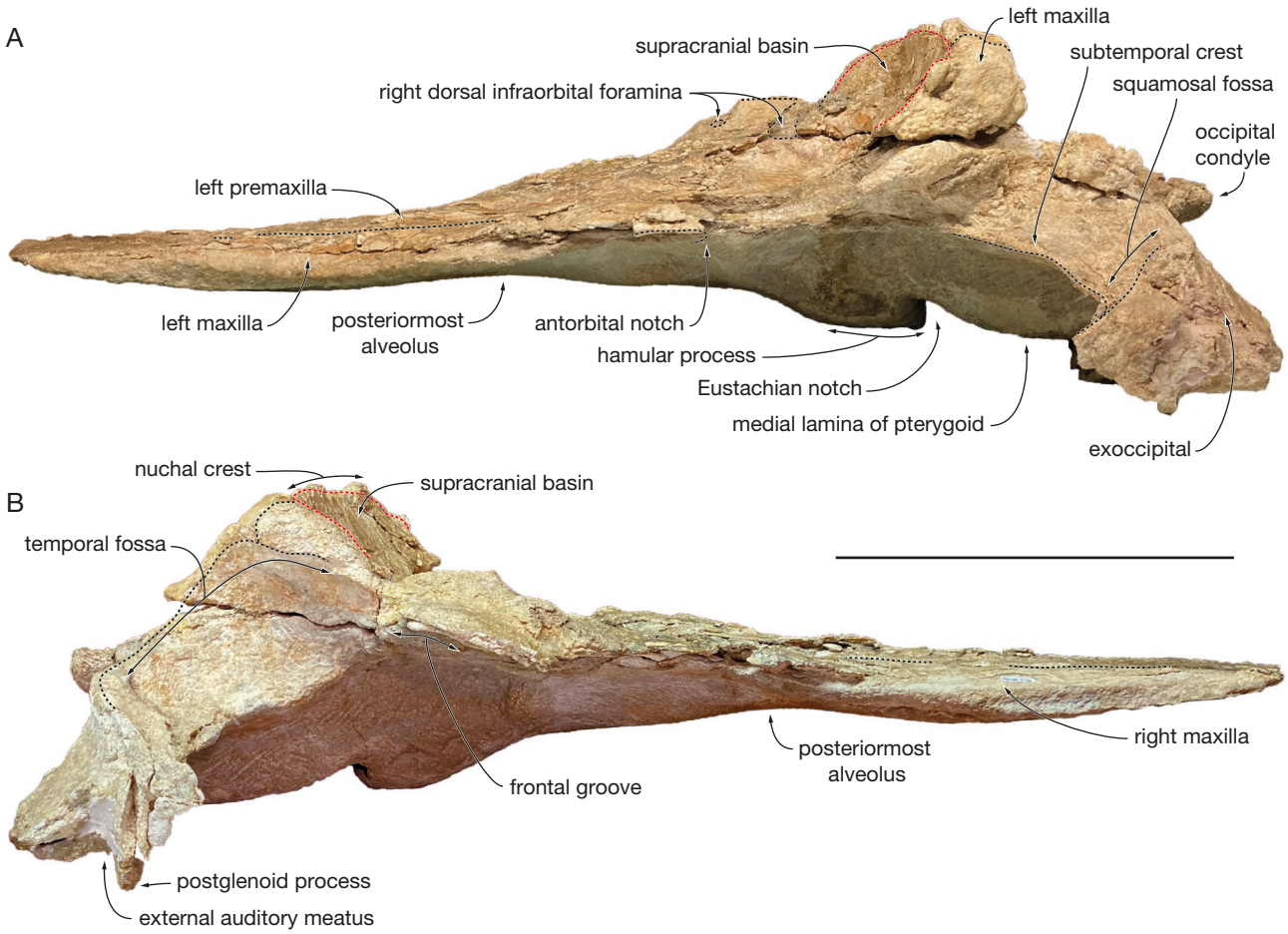

Fig. 4Fig. 4. — Cranium of *Diaphorocetus ortegai* n. sp. MUSM 3246 (holotype, Chilcatay Formation, East Pisco Basin, Peru) in left (**A**) and right (**B**) lateral views. **Black dashed lines** for sutures, foramina, and outline of several bones and temporal fossa; **red dashed line** for posterior outline of supracranial basin. Scale bar: 200 mm.

gests that the supracranial basin did not extend for a long distance along the rostrum base, a condition shared with most other extinct physeteroids. This interpretation is further supported by the proportions of the rostrum, which is tapered in its proximal region, and as such, much narrower than in *Livyatan melvillei* (Lambert, Bianucci, Post, Muizon, Salas-Gismondi, Urbina & Reumer, 2010) and *P. macrocephalus* for its preserved anterior part. As in all other physeteroids, the left bony naris is much larger than the right (ratio between transverse width of right and left naris is estimated at 0.46; Table 1). The right naris is displaced to the left side of the sagittal plane of the skull, in line with the posterior tract of the mesorostral groove.

The preserved anterodorsal roof of the right temporal fossa and parts of the supramastoid crests indicate that the temporal fossae were voluminous, i.e., transversely broad (more than 120 mm) as well as considerably higher dorsoventrally and longer anteroposteriorly than observed in *P. macrocephalus*. Although most of the occipital shield is missing, the anteroposterior position of the non-deformed nuchal crest (markedly anterior to the occipital condyles) indicates that the shield was originally inclined in an anterodorsal direction, drawing an angle of about 45° with the horizontal (Fig. 4).

Premaxilla

Although the dorsal surface of each premaxilla is nearly completely lost along the anterior half of the rostrum, marks of the sutures with the maxillae indicate that the premaxillae did not make the whole dorsal surface of the rostrum in that region, considering the dorsal exposure of the maxillae for a length of at least 310 mm (Fig. 2). The medial edge of the left premaxilla is somewhat better preserved in the proximal portion of the rostrum, attesting to a broad dorsal opening of the mesorostral groove at the rostrum base, with a maximum opening being reached 100 mm anterior to the level of the antorbital notch. It remains unknown whether the right and left premaxillae contacted each other dorsomedially in the anterior part of the rostrum.

The left premaxillary foramen is located just anterior to the level of the antorbital notch, 8.5 mm lateral to the medial margin of the premaxilla, with a transverse diameter of 7 mm (Fig. 2). The foramen marks the posterolateral corner of a short (25 mm long), depressed, and transversely concave surface that may correspond to the prenarial triangle of many non-physeteroid odontocetes. Anterior to this region, the heavily fragmented dorsal surface of the premaxilla is slightly concave transversely for at least 100 mm. Posterior to the premaxillary foramen, the

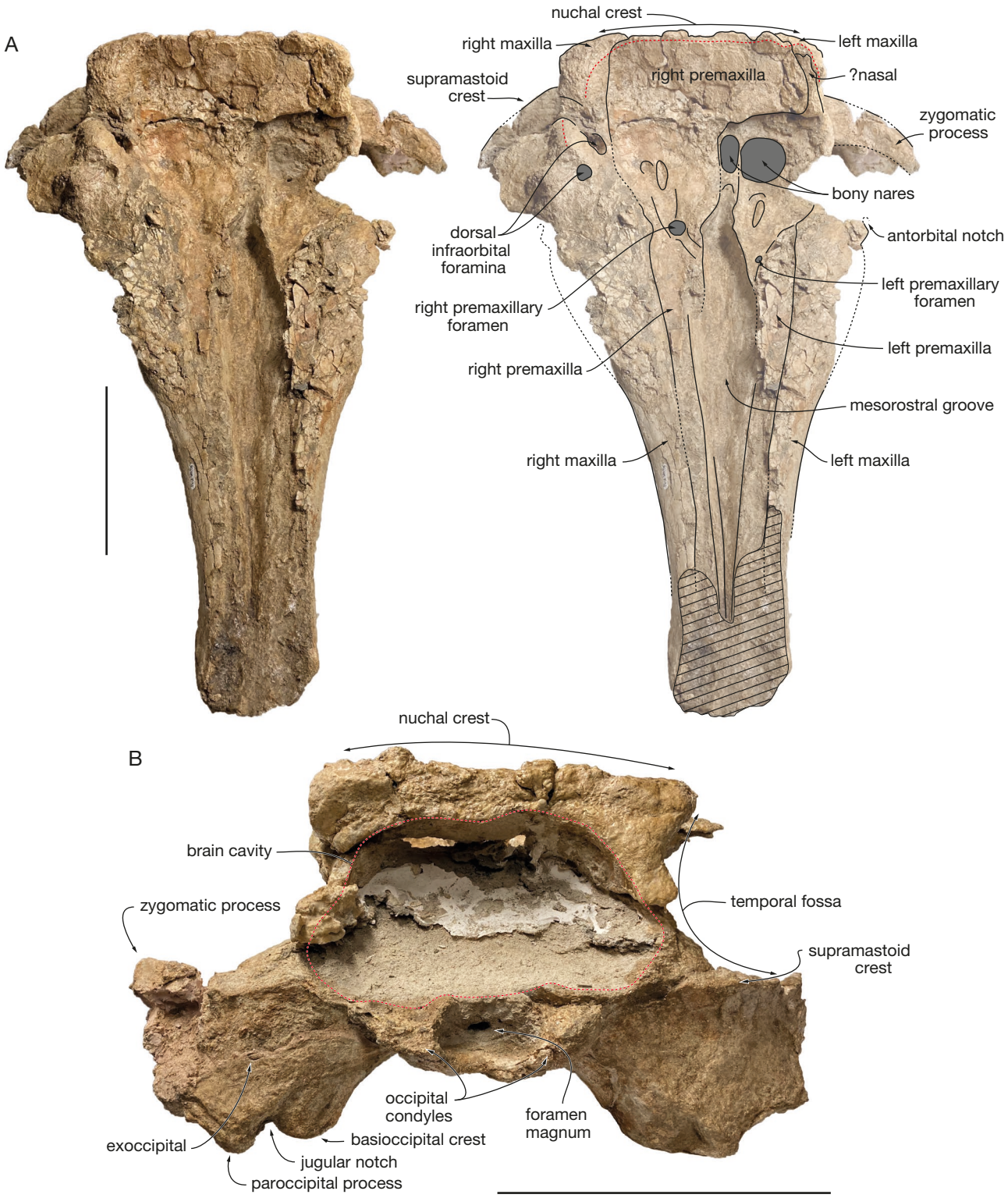

Fig. 5. — Cranium of *Diaphorocetus ortegai* n. sp. MUSM 3246 (holotype, Chilcatay Formation, East Pisco Basin, Peru) in anterodorsal view (**A**) (photo and corresponding line drawing) and posterior view (**B**). Grey shading for sediment; hatching for main break surfaces; black dashed lines for more tentative interpretations of sutures and edges; red dashed lines for posterior outline of supracranial basin and outline of brain cavity. Scale bars: 200 mm.

left premaxilla widens markedly. Its dorsal surface is transversely concave, forming a broad premaxillary sac fossa that is divided by a thick longitudinal ridge for about 43 mm. Medial to this ridge, the fossa is even more concave, with a medial edge raising dorsomedially. At this level, the left premaxilla remains distant from the right, leaving the posterior part of the mesorostral groove dorsally open. Twenty-nine millimeters posterolateral to the left premaxillary foramen, a moderately deep sulcus extends

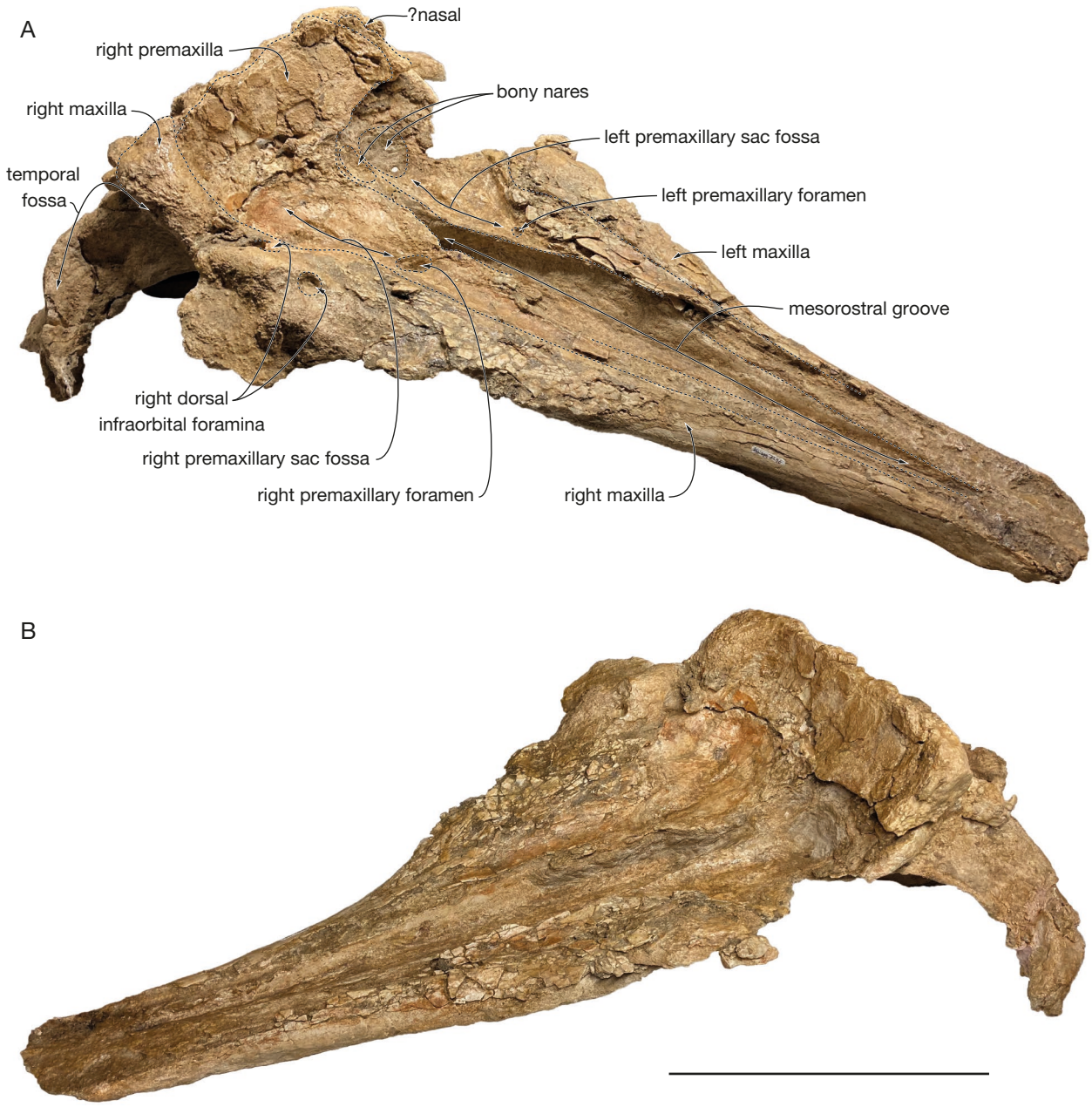

FIG. 6. — Cranium of *Diaphorocetus ortegai* n. sp. MUSM 3246 (holotype, Chilcatay Formation, East Pisco Basin, Peru) in right (**A**) and left (**B**) anterodorsolateral views. Black dashed lines for sutures, foramina, bony nares, and outline of several bones. Scale bar: 200 mm.

obliquely for at least 44 mm and ends parallel to the lateral margin of the premaxilla, being reminiscent of the posterolateral sulcus of non-physeteroid odontocetes (see Lambert *et al.* 2020 for a similar interpretation in *Rhaphicetus valenciae*). The anterior margin of the left bony naris is located shortly posterior to the end of the longitudinal ridge. Posterolaterally, the left premaxilla is incomplete, thus preventing from estimating its extent along the lateral wall of the supracranial basin.

The dorsal surface of the right premaxilla is transversely concave for at least 160 mm anterior to the right premaxillary foramen (Figs 5; 6), a marked difference with the convex premaxilla of *R. valenciae* in this region. The right premaxillary foramen is located 35 mm more posteriorly than the left, shortly behind the proposed level of the antorbital notch; in *Diaphorocetus poucheti*, this foramen is located more anteriorly. The right premaxillary foramen is more than twice larger (transverse diameter 16 mm) than the left. It is followed anteriorly for 36 mm by a well-defined, broad anteromedial sulcus, a feature that was not observed in *R. valenciae*. Another sulcus extends posteriorly from the premaxillary foramen; it is shorter, narrower, and shallower than in the holotype of *R. valenciae*. Smaller depressions mark the right premaxillary sac fossa more posteriorly, including a short and narrow sulcus (29 mm long and 8 mm wide) located medial to a small fossa. Posteromedial to the premaxillary foramen, the surface of the right premaxilla is transversely convex, with a medial edge turning posteromedially towards the presphenoid.

The suture between the right maxilla and premaxilla is difficult to follow in the supracranial basin due to damage in that region; it is estimated that the lateral margin of the premaxilla roughly reaches the medial limit of the largest dorsal infraorbital foramen (see below), at about half the height of the lateral wall of the supracranial basin, having at that level a maximum width of 97 mm. From there, the premaxilla raises onto the posterior wall of the basin, where it contributes to the anteroposteriorly thick nuchal crest, and where the dorsal-most portion of its anteriorly facing surface is vertical. Covering most of the posterior wall of the supracranial basin, the right premaxilla extends far towards the left part of the skull, reaching beyond the lateral margin of the left bony naris (Figs 2; 5), as seen for example in *Cozzuoliphyseter rionegrensis* (Paolucci *et al.* 2021).

On the ventral surface of the rostrum, the two premaxillae are exposed in the anterior part of the median trough, displaying an asymmetric pattern (Fig. 3). The left premaxilla appears 45 mm before the anterior end of the vomer, whereas the right premaxilla remains hidden until a level 50 mm anterior to the vomer, from where it broadens to eventually reach a width similar to that of the left premaxilla at the preserved tip of the rostrum. A similar asymmetry is observed in *D. poucheti*, *P. duboisi*, and *C. rionegrensis*.

Maxilla

The anterior tip of the maxillae is missing, and the abraded dorsal surface makes it difficult to estimate the length of the missing part. Each maxilla is exposed dorsally along the whole preserved length of the rostrum; this exposure widens only slightly for the first 250 mm, followed by a more pronounced widening linked to the broadening of the rostrum towards its base (Figs 2; 5). Using the partly preserved posteromedial wall of the left antorbital notch as a landmark, it is probable that a moderately developed maxillary flange was originally present. In lateral view, the maxillary part of the rostrum is surprisingly thin dorsoventrally for the preserved anterior two thirds of its length (Fig. 4), contributing to the platyrostrine (dorsoventrally flattened) aspect of the rostrum: for example, the maxilla is 32 mm thick 250 mm anterior to the antorbital notch in MUSM 3246, whereas it is 63 mm thick at the same level in the holotype of *Rhaphicetus valenciae*. A similar dorsoventrally flattened maxillary portion of the rostrum is seen in *Diaphorocetus poucheti* (Fig. 7; Paolucci *et al.* 2020) and in the less closely related *Zygophyseter varolai* (Bianucci & Landini 2006).

On the left side, anteromedial to the antorbital notch, the dorsal surface of the maxilla is transversely convex, whereas on the right side it is concave (Figs 5; 6), as in *R. valenciae*. Only the right maxilla is partly preserved in the supraorbital region. It displays two dorsal infraorbital foramina (Figs 2; 5). With a transverse diameter of 9.5 mm and a circular outline, the first such foramen is just posterior to the level of the antorbital notches, being placed at the anterior end of the thick crest that makes the lateral margin of the supracranial basin over the right orbit. The second foramen is larger (anteroposterior diameter estimated at 24 mm), oval in outline, and located 32 mm more posteromedially, along the medial surface of the thick crest. It is followed posterolaterally by a broad sulcus. It cannot be excluded that smaller foramina went unnoticed due to preservation issues on the right side. A large dorsal infraorbital foramen is located more posterodorsally on the right maxilla of the holotype of *D. poucheti*, nearly in line with the nuchal crest. No dorsal infraorbital foramen is preserved on the left side (Fig. 7).

The posterolateral corners of the supracranial basin are mostly made of the maxillae and markedly thickened. Both maxillae extend posteromedially along the nuchal crest for a short distance. Each maxilla ends before the mediolateral level of the corresponding premaxillary foramen, the two maxillae being approximately 120 mm apart.

In ventral view, the left and right maxillae display 18 dental alveoli over a length of 336 mm and 347 mm, respectively (Fig. 3). In addition to maxillary and presumably premaxillary alveoli from the missing anterior section of the rostrum, a few more, shallow alveoli may have been present posteriorly, along the damaged lateral margins of the basal portion of the rostrum. The number of alveoli per 100 mm of alveolar groove length is greater than in *D. poucheti*. The alveolar groove of *Placoziphius duboisi* probably ended more anteriorly compared to MUSM 3246, with shallower posterior alveoli. The right and left anteriormost alveoli are 36.5 mm apart from each other, whereas the right and left posteriormost alveoli are 166 mm from each other, and the last preserved posterior alveolus is 76 mm anterior to the antorbital notch on the left side. The preserved alveoli are well-defined, roughly circular, and deep. They range in transverse diameter from 13 to 18 mm, with the largest occurring at about two thirds of the length of the alveolar groove (13rd to 14th alveoli, numbered from the first preserved anterior alveolus), and the smallest being in the first half (from 4th to 9th along the left alveolar groove). Interalveolar septa range in length from 3 to 18 mm, but most of the septa fall in an interval between 3 and 5.5 mm, with no general trend along the alveolar groove.

Medial to the 17th to 12th right alveoli, five moderately well-defined, subcircular depressions most likely correspond to embrasure pits. The posteriormost such pit is the deepest, with a central part that is 22.5 mm medial to the alveolar groove, and subsequent more anterior pits get gradually shallower. Similar depressions interpreted as embrasure pits have been described medial to the posterior maxillary alveoli in other physeteroids (e.g., *Acrophyseter deinodon*, *D. poucheti*, and *Orycterocetus crocodilinus*), several other odontocetes, and basilosaurids (Lambert *et al.* 2017 and references therein; Paolucci *et al.* 2020). Either the embrasure pits were shallower, or completely absent on the left side, as seen in several pomatodelphinine platanistids (Kellogg 1959; Lambert 2006). The palate is robust, featuring a dorsoventrally thick, 85-mm-wide ventromedial portion of the maxillae with a roughly flat ventral surface, being separated from the transversely concave lateral portions by two parallel crests. Medial to each crest, a deep oblique sulcus is directed anteromedially. The posterior part of each sulcus corresponds to the pterygopalatine canal, which is probably exposed ventrally due to poor preservation of the ventral surface of the maxilla and palatine in this area, whereas the anterior part most likely exited from an unpreserved major palatine foramen.

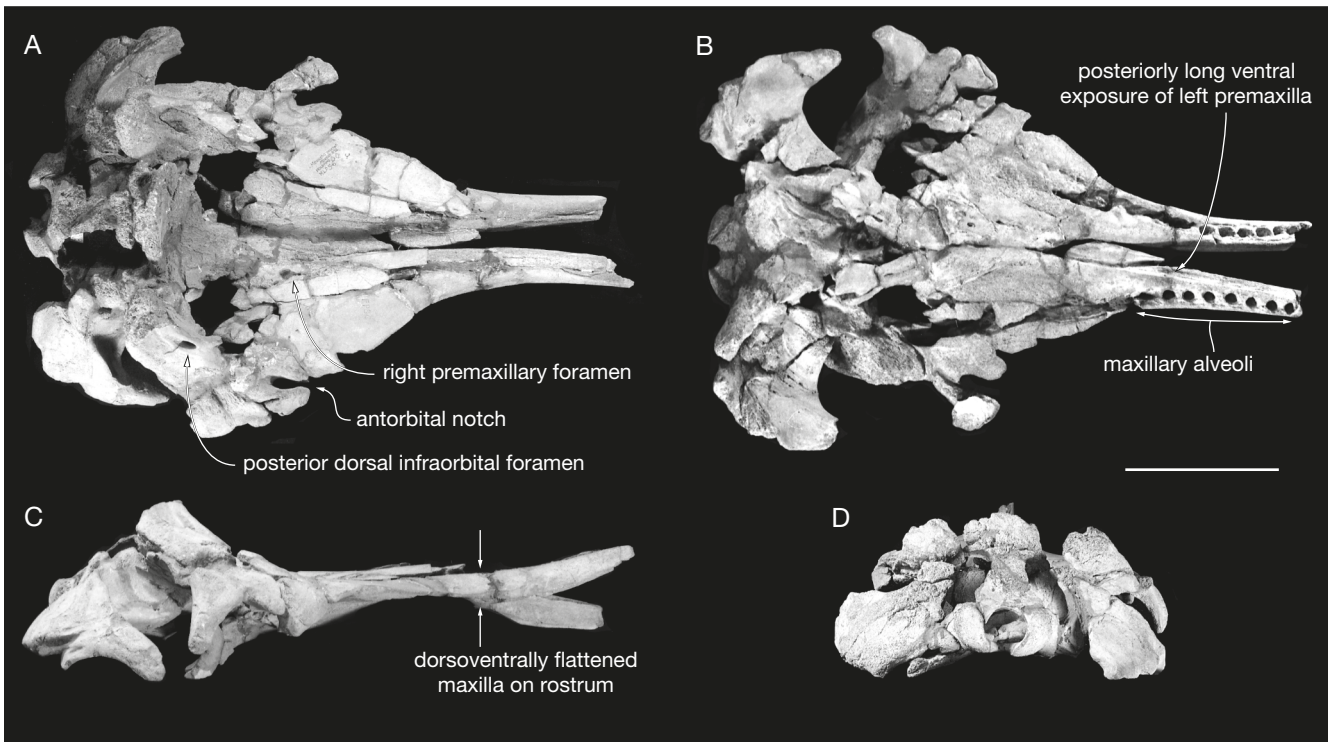

Fig. 7. — Cranium of *Diaphorocetus poucheti* (Moreno, 1892) MLP 5-6 (holotype) in dorsal (**A**), ventral (**B**), right lateral (**C**), and posterior (**D**) views, illustrating among others some diagnostic characters at the genus and species levels. The figured photos were taken by one of us (CM) in 1981, with a preservation state that is closer to the original illustrations in Lydekker (1893), prior to the separation of the right and left rostral parts and pterygoids/palatines from the neurocranium and with more complete antorbital notches and right orbit. Scale bar: 200 mm.

Vomer

Ventrally, the vomer is exposed along the median trough for 180 mm, starting from a level 56 mm anterior to the antorbital notches, and reaching a maximum width of 28 mm (Fig. 3). From this level forward, the ventral surface of the vomer becomes keeled. Posterior to the choanae, the sutures of the vomer with other bones in the basioccipital basin could not be clearly detected due to damaged bone surfaces and partial covering by sediment.

Palatine and pterygoid

Part of the maxilla-palatine suture is visible on the right side, leaving the sagittal plane of the skull in an anterolateral direction from a level 35 mm posterior to the antorbital notch (Fig. 3). The anterior tip of the right palatine is about 25 mm anterior to the level of the antorbital notch. The anterolateral portion of each pterygoid can be outlined as a narrow (15 mm wide) plate participating to the anteromedial edge of the pterygoid sinus fossa. This edge rapidly becomes poorly defined lateral to the anterior tip of the pterygoid, which is located posterior to the level of the antorbital notch, ending 55 mm posterior to the apex of the palatine. Ventromedially defining the broad pterygoid sinus fossae, the hamular processes of the pterygoids are massive, with a maximum joined width of 58 mm and a depressed median region. The posterior tips of the right and left pterygoids are joined and project for 25 mm posterior to the bottom of the Eustachian notches. The medial lamina of the pterygoid makes a long portion (117 mm on the left side) of the lateral wall of the basioccipital basin. Being slender anteriorly, it gradually thickens posterolaterally to reach a transverse thickness of 21 mm.

Presphenoid

In dorsal view, the presphenoid is only visible for a short distance between the posterior end of the mesorostral groove and the right bony naris (Figs 2; 5). Details of the relationships with the vomer and premaxillae cannot be distinguished.

Nasal

Along the left lateral margin of the right premaxilla, on the left posterolateral corner of the supracranial basin, a narrow and thin plate of bone is tentatively interpreted as part of a single nasal bone (Figs 2; 5).

Frontal

Dorsally, apart from the exposure of part of the right supraorbital process due to removal of the overlying maxilla, frontals are thought to appear only along the thick nuchal crest, in the section separating the two maxillae, between the left premaxilla and small fragments of the supraoccipital (Fig. 2). The only feature of the frontal that is visible in ventral view is the narrow medial portion of the right frontal groove, which is obliquely oriented to form an angle of about 45° with the sagittal plane of the cranium (Fig. 3).

Occipital shield and brain cavity
No part of the supraoccipital is preserved, leaving the brain cavity open (Figs 2; 5). The latter has a preserved maximum width of 210 mm, in its lower half; it is markedly wider than high, a condition that most likely reflects the shape of the brain, as seen for example in *Kogia sima* Owen, 1866 and *Physeter macrocephalus* (Flower 1867; Ries & Langworthy 1937; Marino *et al.* 2003). The minimum distance between the temporal fossae across the occipital region makes less than 43 % of the bizygomatic width (Table 1), corresponding to a relatively narrow occipital shield, laterally margined by transversely broad temporal fossae. The shield is dorsoventrally low, as testified by the low position of the nuchal crest (see above), hence a stocky posterior outline of the skull.

Squamosal
In dorsal view, the preserved part of each zygomatic process is directed anterolaterally, before gradually turning to a more anterior direction (Fig. 2). Considering the direction of the anterior part of the zygomatic process in other physeteroids with a long temporal fossa, it is estimated that a large part of each zygomatic process (at least 90 mm on the right side) is missing. The supramastoid crest raises posterodorsomedially, as in other physeteroids (Fig. 4). The right postglenoid process is partly preserved, making a slightly obliquely directed thin plan (thickness 8-9 mm) and reaching farther ventrally than the posttympanic process, as in *Diaphorocetus poucheti*. In ventral view, the left falciform process has a triangular outline, with a dorsoventrally thin ventromedial tip (Fig. 3). Part of the tympanosquamosal recess is better seen on the right side, medial to the postglenoid process, and extending anterolaterally along the damaged mandibular fossa.

Alisphenoid
Finely preserved on the left side, the ventral suture between alisphenoid and squamosal zigzags in an anterolateral direction, reaching the subtemporal crest some distance anteromedial to the anterior most edge of the squamosal fossa (Fig. 3). Filled with hardened sediment on both sides, the foramen ovale is followed laterally by a wide and shallow path for the mandibular nerve (V3), which gradually turns more anteriorly, disappearing before the subtemporal crest. Anterior to this path, the ventral surface of the alisphenoid is approximatively flat, sloping anterodorsolaterally.

Exoccipital
The posterior surface of the exoccipital slopes posteroventrally, with an angle of 45-50° with the horizontal plane (Fig. 4). Only the ventral part of the occipital condyles is preserved, being lower than the posteroventral margin of the temporal fossae (Fig. 5). The condyles protrude moderately from the neurocranium, reaching posteriorly just beyond the ventral margin of the exoccipitals. The ventral surface of the paroccipital process is deeply excavated, with a laterally directed broad groove (better preserved on the left exoccipital) (Fig. 3). Anterolateral to the left paroccipital process, a broad and dorsoventrally thin piece of bone ventrally marked by laterally directed grooves and ridges is tentatively interpreted as part of the posterior process of the left tympanic bulla.

Basioccipital
Though the basioccipital basin is anteroposteriorly long (147 mm from the posterior tip of the hamular processes), the contribution of the basioccipital crests to its dorsolateral walls is relatively limited (see medial lamina of pterygoid above) (Fig. 3). The dorsal surface of the basioccipital basin is markedly anteroposteriorly convex. The posterolateral portion of each basioccipital crest is robust (maximum transverse thickness equaling 38 mm on the left side), medially defining a moderately deep and broad jugular notch.

PHYLOGENY

The heuristic search yielded 1584 most parsimonious trees with a length of 184 steps, a consistency index of 0.46 and a homoplasy index of 0.54. The strict consensus tree is shown in Figure 8. This tree is less resolved than that presented by Peri *et al.* (2022b), with more uncertainty for the relationships of *Cozzuoliphyseter rionegrensis*, *Diaphorocetus poucheti*, and *Placoziphius duboisi*. Though *C. rionegrensis* is recovered as a stem physeteroid, as in Peri *et al.* (2022b), *D. poucheti* and *P. duboisi* shift here from crown physeteroids to stem physeteroids, a result that agrees with part of the trees obtained by Paolucci *et al.* (2020). MUSM 3246 falls as the sister-group of *D. poucheti*. The Adams consensus tree (Fig. 8, inset) differs only from the strict consensus tree in the partly resolved relationships between *Diaphorocetus* spp., *C. rionegrensis*, and *P. duboisi*, these taxa forming a previously never recovered clade, including at least three Early Miocene stem physeteroids. These relationships were recovered in the analysis with down-weighting of homoplastic characters (k = 3); there, *Diaphorocetus* spp., *C. rionegrensis*, and *P. duboisi* also form a clade of stem physeteroids, with *P. duboisi* being sister-group to *Diaphorocetus* spp. (Appendix 5).

DISCUSSION

Systematics and phylogeny

Among extinct physeteroids, MUSM 3246 shares the following similarities with *Cozzuoliphyseter rionegrensis*, *Diaphorocetus poucheti* (both of which originating from the Miocene of the southwestern Atlantic), and *Placoziphius duboisi* (from the Early Miocene of the North Sea): asymmetric exposure of the premaxillae between the maxillae on the ventral surface of the rostrum, with the right premaxilla being wider and posteriorly longer than the left (char. 58, state 2); and right posterolateral margin of the supracranial basin being angular in dorsal view (char. 57, state 1, also seen in *Aulophyseter morricei*). These shared morphological features may indicate close relationships between MUSM 3246, *C. rionegrensis*, *D. poucheti*, and *P. duboisi*, all of which are recovered in our phylogenetic analysis as stem physeteroids. In addition to the many similarities pointed out in the description above, MUSM 3246 shares with *D. poucheti* one key feature, i.e., the dorsoventral flattening of the maxillary portion of the rostrum (ratio between maximum dorsoventral height of maxilla along the anterior half

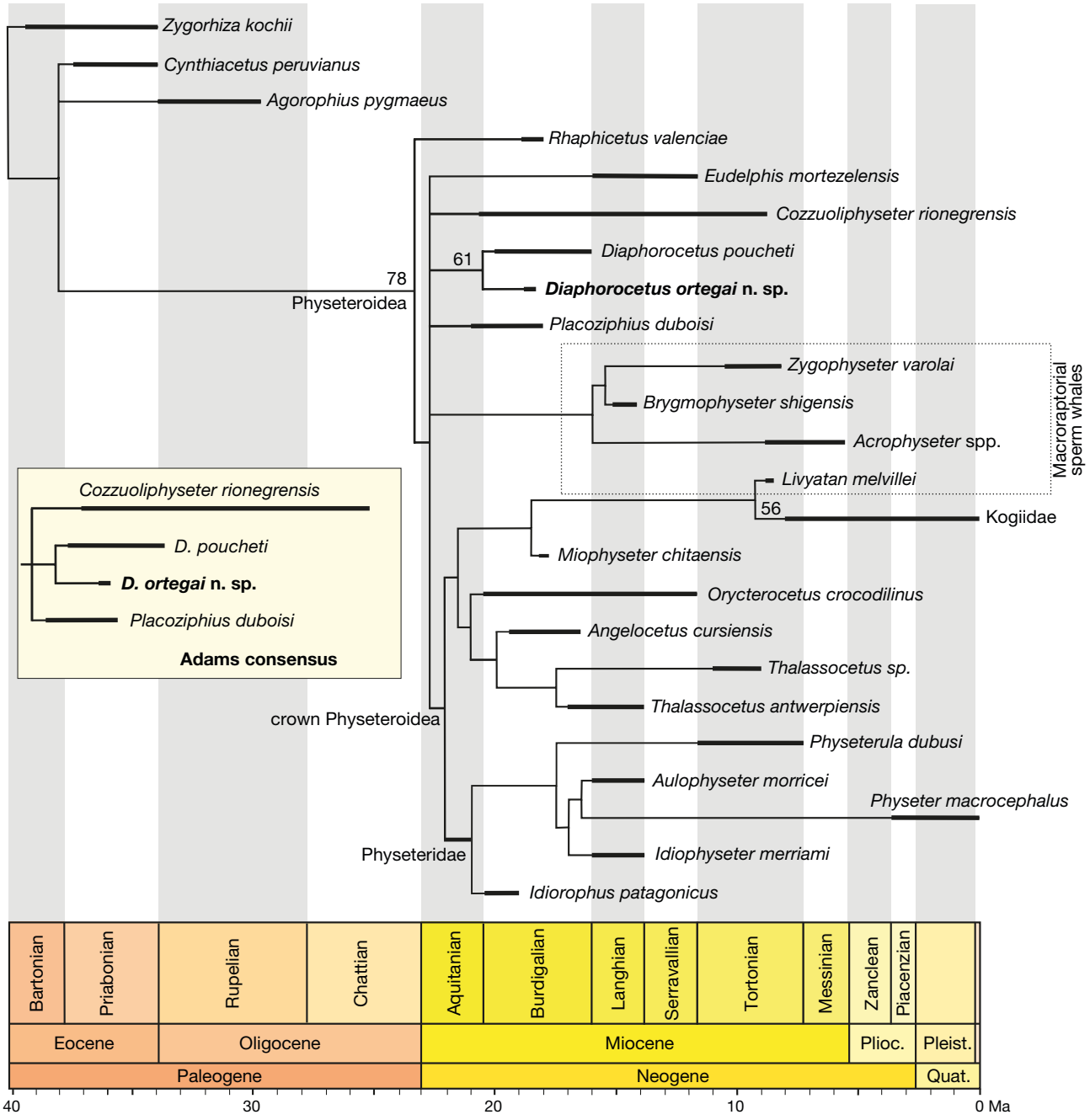

FIG. 8. — Time-calibrated strict consensus tree of 1584 most parsimonious trees with a length of 184 steps, a consistency index of 0.46, and a homoplasy index of 0.54, resulting from the analysis with equal-weighting, describing the sister-group relationship between *Diaphorocetus poucheti* (Moreno, 1892) and *Diaphorocetus ortegai* n. sp. among stem Physeteroidea. Relationships within Kogiidae are collapsed. Bootstrap values higher than 50 are indicated at nodes. Inset: part of the Adams consensus tree illustrating partly resolved relationships between *Cozzuoliphyseter rionegrensis* (Gondar, 1975), *Diaphorocetus* spp., and *Placoziphius duboisi* Van Beneden, 1869. See the Material and methods section for information on chronostratigraphic ranges.

of the rostrum and bizygomatic width lower than 0.1; char. 55, state 1). As illustrated by the sister-group relationship recovered by our two phylogenetic analyses, these similarities support the attribution of MUSM 3246 to the genus *Diaphorocetus*. It should be noted that the more fragmentarily preserved rostrum of the holotype of *Miophyseter chitaenensis* may also bear dorsoventrally flattened maxillae (Kimura & Hasegawa, 2023); however, more complete material of this other Early Miocene physeteroid is needed to allow for a detailed comparison.

The main differences with the type of *D. poucheti* (Fig. 7) are: smaller cranial dimensions, a higher number of maxillary alveoli per length unit, the right premaxillary foramen being posterior to the level of the antorbital notch, and the absence of a large dorsal infraorbital foramen in the posterodorsal region of the right maxilla. While the holotype of *D. poucheti* is interpreted as representing a subadult individual (Paolucci *et al.* 2020) and MUSM 3246 a subadult to adult, allowing for a size comparison that is possibly not

too impacted by ontogeny, size differences alone should still be used with caution (considering for example the major size differences observed between adult males and females of the extant great sperm whale *Physeter macrocephalus*; Rice 1989). Nevertheless, considering the intraspecific variations that occur in extant physeteroids, and more generally in extant odontocetes, the above combination of differences is considered sufficient to diagnose a new species within the genus *Diaphorocetus*. Additional, more complete specimens from both coasts of South America will hopefully allow further testing of this interpretation.

Because *D. poucheti* is known by a single specimen (Paolucci *et al.* 2020), the description of *Diaphorocetus ortegai* n. sp. may help clarifying some aspects of the cranial anatomy of the former. Indeed, the relative position of the different cranial elements remains poorly constrained in the type of *D. poucheti*. Firstly, the rostrum and pterygoids are now detached from the neurocranium. Secondly, ancient reconstructions of the different elements of the neurocranium remain questionable. Unfortunately, the medial region does not show clear bony contacts with the lateral parts, including portions of the squamosals and exoccipitals; as a result, the zygomatic processes of the squamosals point in an anteroventral direction that appears highly unusual for a toothed cetacean and may be difficult to understand from a functional viewpoint (concerning the articulation of the mandible). A reassessment of the orientation of the squamosals and a more accurate positioning of the detached elements of the cranium of this specimen would possibly benefit from a comparison with MUSM 3246, which unfortunately misses a large part of its zygomatic processes.

Palaeobiology

The relatively high number of well-defined dental alveoli (more than 18 per upper quadrant) in both the upper and lower jaws (as indicated by the presence of embrasure pits in the maxilla), coupled with their diameter proportionally smaller than in macroraptorial sperm whales (Boersma & Pyenson 2015; Lambert *et al.* 2017), indicates that *Diaphorocetus ortegai* n. sp. was able to prey upon small to medium-sized fish, which it most likely grasped with its teeth, as proposed for *Diaphorocetus poucheti* (Paolucci *et al.* 2020). Compared to *Rhaphicetus valenciae*, a similarly sized physeteroid also occurring in the *Ct1a* strata of the Chilcatay Formation, which also displays an elongated rostrum and no clear osteological adaptations for suction feeding (Lambert *et al.* 2020), *D. ortegai* n. sp. has a maxillary portion of the rostrum that is considerably flattened dorsoventrally, contrasting with the roughly cylindrical rostrum of *R. valenciae* (Fig. 9). Also present in *D. poucheti* (Fig. 7), this character may indicate a somewhat different prey capture technique for *Diaphorocetus* spp. Similar differences in rostral cross-section observed in hyper-longirostrine dolphins were interpreted in a kinematic disparity context to facilitate different types of movements: for example, with their dorsoventrally flattened (and thus mediolaterally reinforced) rostra, Miocene pomatodelphinine platanistids were proposed to perform more lateral sweeps for the capture of prey, compared to taxa with a more cylindrical or transversely flattened rostrum (McCurry & Pyenson 2019). A similar interpretation could be done for the platyrostrine *D. ortegai* n. sp. and *D. poucheti*, whereas *R. valenciae* may have performed sweeps in a wider range of directions with the robust, presumably edentulous anterior part of its upper jaw (Lambert *et al.* 2020) – a difference that could have led to some degree of niche partitioning between these two contemporaneous, similarly sized, likely sympatric physeteroid taxa. Different feeding strategies may have allowed for the capture of slightly different prey types or for predation in different environments (e.g., closer to the seafloor in the more laterally sweeping *D. ortegai* n. sp.). That said, our new species further supports the observation that Burdigalian physeteroids are all to be classified as generalist raptorial feeders and occupied a relatively narrow interval of body sizes, while the first cranial clues for macroraptorial and suction-feeding species only appear during the Langhian, and are paralleled by an increase in the range of body sizes that will further expand during the Late Miocene with the appearance of kogiids (Peri *et al.* 2022b).

With the exception of *R. valenciae*, *D. ortegai* n. sp. was distinctly larger than all other odontocetes from the Burdigalian part of the Chilcatay Formation, even larger than the squalodelphinid *Macrosqualodelphis ukupachai* Bianucci, Bosio, Malinverno, Muizon, Villa, Urbina & Lambert, 2018 and the heterodont dolphin *Inticetus vertizi* Lambert, Muizon, Malinverno, Di Celma, Urbina & Bianucci, 2018 (Bianucci *et al.* 2018a; Lambert *et al.* 2018). In addition, the diameter of the maxillary alveoli of *M. ukupachai* falls in the lower part of the range measured in *D. ortegai* n. sp., and the dimensions of the incisors and canines of *I. vertizi* also correspond to slightly smaller alveoli. *D. ortegai* n. sp. may thus have been able to target larger prey than most other co-occurring cetaceans, while using a different feeding technique compared to *R. valenciae*. Nevertheless, *D. ortegai* n. sp. was probably not the apex predator of the Chilcatay palaeoenvironment – a role that in all likelihood pertained to the large-bodied otodontid shark *Carcharocles chubutensis* (Ameghino, 1906) (Bianucci *et al.* 2018b).

Palaeobiogeography

The description of a new species of the genus *Diaphorocetus*, which was previously only known from the Burdigalian of Argentina, calls for updating the comparisons between the odontocete assemblages of the Peruvian Chilcatay Formation and the roughly synchronous late Early Miocene Gaiman and Monte Leon formations of Argentinian Patagonia (Viglino *et al.*, 2021; Cuitiño *et al.* 2023). These assemblages share the occurrence of: two medium-sized physeteroids (*Diaphorocetus ortegai* n. sp. and *Rhaphicetus valenciae* vs *Diaphorocetus poucheti* and *Idiorophus patagonicus* (Lydekker, 1893)); a relatively large, long-snouted heterodont odontocete (*Inticetus vertizi* vs *Phoberodon arctirostris* Cabrera, 1926); at least one medium-sized, long-snouted homodont dolphin (*Chilcacetus cavirhinus* and eurhinodelphinids vs

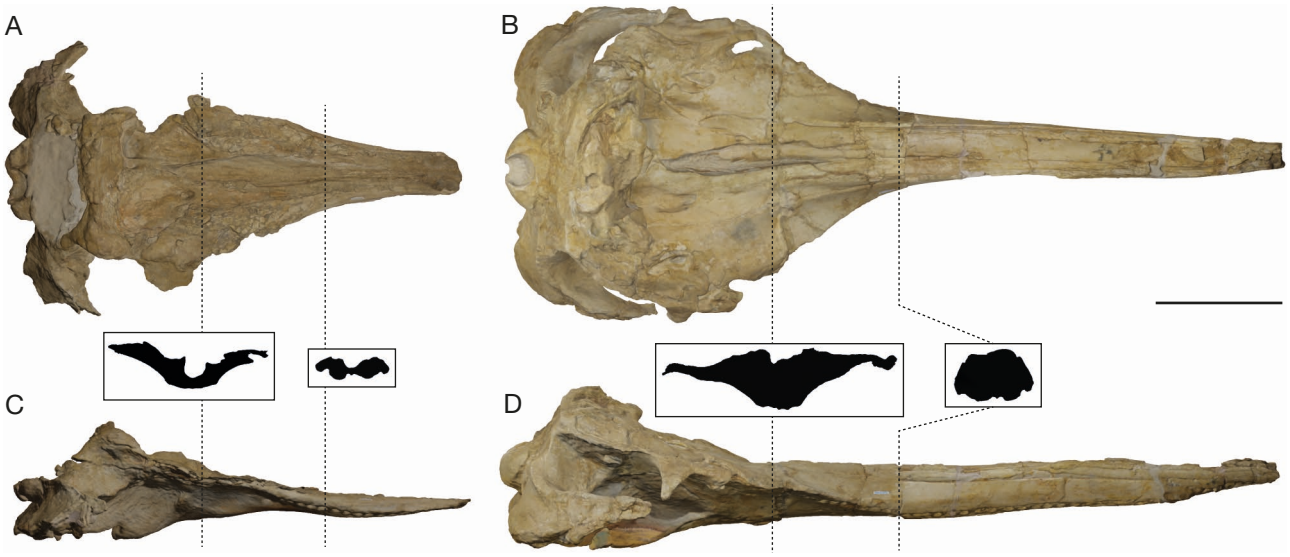

Fig. 9. — Comparison of the crania of *Diaphorocetus ortegai* n. sp. MUSM 3246 (holotype) (**a, c**) and *Rhaphicetus valenciae* Lambert, Muizon, Urbina & Bianucci, 2020 MUSM 2543 (holotype) (**B, D**), both from the Chilcatay Formation (East Pisco Basin, Peru), in dorsal (**A, B**) and right lateral (**C, D**) views, based on 3D models resulting from surface-scanning (see Appendices 1; 2), illustrating the difference in the cross-section of the maxillae on the rostrum (much more dorsoventrally flattened in *D. ortegai* n. sp.). Note that most of the premaxillae is lost on the rostrum of the holotype of *D. ortegai* n. sp., truncating the dorsal part of the anterior cross-sections. Scale bar: 200 mm.

Argyrocetus patagonicus Lydekker, 1893); a medium-sized squalodelphinid (possibly the same species, *Notocetus vanbenedeni*, but see Viglino *et al.*, 2022 for an alternative interpretation); and a small kentriodontid (*Kentriodon* sp.) (Lydekker 1893; Bianucci *et al.* 2018b; Cuitiño *et al.* 2019; Paolucci *et al.* 2020; Bianucci *et al.* 2020; Lambert *et al.* 2021; Viglino *et al.* 2019, 2021, 2022).

Strengthening previous suggestions of vertebrate faunal flow between the Chilcatay palaeobiotopes and the Atlantic realm (Peri *et al.* 2019; Collareta *et al.* 2022), the shared presence of the genera *Diaphorocetus* and *Notocetus* Moreno, 1892 evokes the existence of a dispersal route between the east and west coasts of South America during the Early Miocene (note that the genus *Kentriodon* Kellogg, 1927 is more widely distributed, so that its South American records do not imply any specific biogeographic link; Kimura & Hasegawa 2019). Furthermore, the many morphotypes shared by the Chilcatay and Gaiman/Monte Leon cetacean assemblages may point to similarities in the structuring of the local odontocete communities. This may be due to the existence of relatively similar oceanographic and palaeoenvironmental conditions along the southwestern and southeastern sides of South America (Di Celma *et al.* 2018, 2019; Cuitiño *et al.* 2019; Viglino *et al.* 2021) prior to the Late Miocene strengthening of the Humboldt Current and the consequent emergence of the modern upwelling system along the Pacific South American coast (Bosio *et al.* 2020; Collareta *et al.* 2021; Ochoa *et al.* 2021; Kiel *et al.* 2023).

Together with new discoveries in the field, further comparisons focusing on the Middle to Late Miocene time interval may reveal when and how the similarities between cetacean faunas from the southwestern Atlantic and southeastern Pacific decreased and/or fluctuated until the modern-day situation. A broader comparison with Miocene physeteroid faunas from the Northern Hemisphere (e.g., Atlantic Coastal Plain, Mediterranean, North Sea, and North Pacific) may also contribute to an improved knowledge of sperm whale distribution, dispersal routes, and paleoecology during the heydays of this superfamily. For example, no physeteroids have been reported to date from the Lower Miocene of the northeastern Pacific, while this region has yielded squalodelphinid and early delphinidan records (e.g., Nelson & Uhen, 2018; Peredo *et al.* 2018).

Acknowledgements

We wish to thank Rafael Varas-Malca and Walter Aguirre for their help during fieldwork in the East Pisco Basin, especially when excavating and collecting the fossil specimen studied here, Walter Aguirre for fossil preparation, David J. Bohaska, Sébastien Bruaux, Mónica Buono, Simone Farina, Marta Fernández, John J. Ososky, Florencia Paolucci, Olivier Pauwels, Nicholas D. Pyenson, Rodolfo Salas-Gismondi, Chiara Sorbini, and Rafael Varas-Malca for providing access to collections, and Florencia Paolucci for providing photos of Argentinian physeteroid fossils. We would like to thank the three reviewers, Toshiyuki Kimura, Florencia Paolucci, and Jorge Vélez-Juarbe, as well as the editor Emmanuel Côtez, for their many useful suggestions that improved a previous draft of this work. The PhD thesis of A.B.-P. at the University of Zürich is funded by a Candoc Grant (FK-22-082). The stay of R.B. at the MUSM has been funded by a Stan Wood Award from the Palaeontological Association (United Kingdom). The research of AC, MM and GB is supported by a grant from the Italian Ministero dell'Università e della Ricerca (PRIN Project 2022MAM9ZB).

REFERENCES

Acosta Hospitaleche C. & Stucchi M. 2005. — Nuevos restos terciarios de Spheniscidae (Aves, Sphenisciformes) procedentes de la costa del Perú. *Revista Española de Paleontología* 20 (1): 1-5.

Alfsen A., Bosselaers M. & Lambert O. 2021. — New sperm whale remains from the late Miocene of the North Sea and a revised family attribution for the small crown physeteroid *Thalassocetus* Abel, 1905. *Comptes Rendus Palevol* 20 (39): 807-822. https://doi.org/10.5852/cr-palevol2021v20a39

Benites-Palomino A., Vélez-Juarbe J., Salas-Gismondi R. & Urbina M. 2020. — *Scaphokogia totajpe*, sp. nov., a new bulky-faced pygmy sperm whale (Kogiidae) from the late Miocene of Peru. *Journal of Vertebrate Paleontology*: e1728538. https://doi.org/10.1080/02724634.2019.1728538

Benites-Palomino A., Vélez-Juarbe J., Collareta A., Ochoa D., Altamirano A., Carré M., Laime M. J., Urbina M. & Salas-Gismondi R. 2021. — Nasal compartmentalization in Kogiidae (Cetacea, Physeteroidea): insights from a new late Miocene dwarf sperm whale from the Pisco Formation. *Papers in Palaeontology* 7 (3): 1507-1524. https://doi.org/10.1002/spp2.1351

Bianucci G. & Collareta A. 2022. — An overview of the fossil record of cetaceans from the East Pisco Basin (Peru). *Bolletino de la Società Paleontologica Italiana* 61: 19-60. https://doi.org/10.4435/BSPI.2022.04

Bianucci G. & Landini W. 2006. — Killer sperm whale: a new basal physeteroid (Mammalia, Cetacea) from the Late Miocene of Italy. *Zoological Journal of the Linnean Society* 148: 103-131. https://doi.org/10.1111/j.1096-3642.2006.00228.x

Bianucci G., Bosio G., Malinverno E., Muizon C. de, Villa I. M., Urbina M. & Lambert O. 2018a. — A new large squalodelphinid (Cetacea, Odontoceti) from Peru sheds light on the Early Miocene platanistoid disparity and ecology. *Royal Society Open Science* 5 (4): 172302. https://doi.org/10.1098/rsos.172302

Bianucci G., Collareta A., Bosio G., Landini W., Gariboldi K., Gioncada A., Lambert O., Malinverno E., Muizon C. de, Varas-Malca R., Villa I. M., Coletti G., Urbina M. & Di Celma C. 2018b. — Taphonomy and palaeoecology of the lower Miocene marine vertebrate assemblage of Ullujaya (Chilcatay Formation, East Pisco Basin, southern Peru). *Palaeogeography, Palaeoclimatology, Palaeoecology* 511: 256-279. https://doi.org/10.1016/j.palaeo.2018.08.013

Bianucci G., Muizon C. de, Urbina M. & Lambert O. 2020. — Extensive diversity and disparity of the Early Miocene platanistoids (Cetacea, Odontoceti) in the southeastern Pacific (Chilcatay Formation, Peru). *Life* 10 (3): 27. https://doi.org/10.3390/life10030027

Bianucci G., Urbina M. & Lambert O. 2015. — A new record of *Notocetus vanbenedeni* (Squalodelphinidae, Odontoceti, Cetacea) from the early Miocene of Peru. *Comptes Rendus Palevol* 14 (1): 5-13. https://doi.org/10.1016/j.crpv.2014.08.003

Bloodworth B. & Marshall C. D. 2005. — Feeding kinematics of *Kogia* and *Tursiops* (Odontoceti: Cetacea): characterization of suction and ram feeding. *The Journal of Experimental Biology* 208: 3721-3730. https://doi.org/10.1242/jeb.01807

Boersma A. T. & Pyenson N. D. 2015. — *Albicetus oxymycterus*, a new generic name and redescription of a basal physeteroid (Mammalia, Cetacea) from the Miocene of California, and the evolution of body size in sperm whales. *PLoS ONE* 10 (12): e0135551. https://doi.org/10.1371/journal.pone.0135551

Bosio G., Bianucci G., Collareta A., Landini W., Urbina M. & Di Celma C. 2022. — Ultrastructure, composition, and $^{87}Sr/^{86}Sr$ dating of shark teeth from lower Miocene sediments of southwestern Peru. *Journal of South American Earth Sciences* 118: 103909. https://doi.org/10.1016/j.jsames.2022.103909

Bosio G., Collareta A., Di Celma C., Lambert O., Marx F.G., Muizon C. de, Gioncada A., Gariboldi K., Malinverno E., Varas-Malca R., Urbina M. & Bianucci G. 2021. — Taphonomy of marine vertebrates of the Pisco Formation (Miocene, Peru): Insights into the origin of an outstanding Fossil-Lagerstätte. *PLoS ONE*, 16: e0254395. https://doi.org/10.1371/journal.pone.0254395

Bosio G., Malinverno E., Collareta A., Di Celma C., Gioncada A., Parente M., Berra F., Marx F. G., Vertino A., Urbina M. & Bianucci G. 2020. — Strontium Isotope Stratigraphy and the thermophilic fossil fauna from the middle Miocene of the East Pisco Basin (Peru). *Journal of South American Earth Sciences* 97: 102399. https://doi.org/10.1016/j.jsames.2019.102399

Buono M. R., Fernández M. S., Cozzuol M. A., Cuitiño J. I. & Fitzgerald E. M. 2017. — The early Miocene balaenid *Morenocetus parvus* from Patagonia (Argentina) and the evolution of right whales. *PeerJ* 5: e4148. https://doi.org/10.7717/peerj.4148

Coletti G., Bosio G., Collareta A., Buckeridge J., Consani S. & El Kateb A. 2018. — Palaeoenvironmental analysis of the Miocene barnacle facies: case studies from Europe and South America. *Geologica Carpathica* 69 (6): 573-592. https://doi.org/10.1515/geoca-2018-0034

Collareta A., Lambert O., Muizon C. de, Urbina M. & Bianucci G. 2017. — *Koristocetus pescei* gen. et sp. nov., a diminutive sperm whale (Cetacea: Odontoceti: Kogiidae) from the late Miocene of Peru. *Fossil Record* 20: 259-278. https://doi.org/10.5194/fr-20-259-2017

Collareta A., Lambert O., Muizon C. de, Benites Palomino A. M., Urbina M. & Bianucci G. 2020. — A new physeteroid from the late Miocene of Peru expands the diversity of extinct dwarf and pygmy sperm whales (Cetacea: Odontoceti: Kogiidae). *Comptes Rendus Palevol* 95 (5): 79-100. https://doi.org/10.5852/cr-palevol2020v19a5

Collareta A., Lambert O., Marx F. G., Muizon C., De, Varas-Malca R., Landini W., Bosio G., Malinverno E., Gariboldi K., Gioncada A., Urbina M. & Bianucci G. 2021. — Vertebrate palaeoecology of the Pisco Formation (Miocene, Peru): glimpses into the ancient Humboldt Current ecosystem. *Journal of Marine Science and Engineering* 9 (11): 1188. https://doi.org/10.3390/jmse9111188

Collareta A., Kindlimann R., Baglioni A., Landini W., Sarti G., Altamirano A., Urbina M. & Bianucci G. 2022. — Dental morphology, palaeoecology and palaeobiogeographic significance of a new species of requiem shark (genus *Carcharhinus*) from the Lower Miocene of Peru (East Pisco Basin, Chilcatay Formation). *Journal of Marine Science and Engineering* 10 (10): 1466. https://doi.org/10.3390/jmse10101466

Collareta A., Carnevale G., Bianucci G., Varas-Malca R., Altamirano-Sierra A., Urbina M. & Di Celma C. 2023. — A puzzling occurrence of the bite mark ichnogenus Linichnus from the Lower Miocene Chilcatay Formation of Peru. *Neues Jahrbuch für Geologie und Paläontologie, Abhandlungen* 308 (2): 171-180. https://doi.org/10.1127/njgpa/2023/1135

Cuitiño J. I., Buono M. R., Viglino M., Farroni N. D. & Bessone S. 2019. — Factors affecting the preservation and distribution of cetaceans in the lower Miocene Gaiman Formation of Patagonia, Argentina. *Palaeogeography, Palaeoclimatology, Palaeoecology* 526: 110-125. https://doi.org/10.1016/j.palaeo.2019.03.013

Cuitiño J. I., Bilmes A., Buono M. R., Bordese S., Herazo L. & Scasso R. A. 2023. — Stratigraphy, provenance, and timing of Neogene sedimentation in the western Valdés Basin, Patagonia. Accurate paleogeographic reconstructions as a key piece for andean-passive margin integration. *Journal of South American Earth Sciences*: 104278. https://doi.org/10.1016/j.jsames.2023.104278

DeVries T. & Jud N. 2018. — Lithofacies patterns and paleogeography of the Miocene Chilcatay and lower Pisco depositional sequences (East Pisco Basin, Peru). *Boletín de la Sociedad Geológica del Perú* 8: 124-167.

DeVries T. J., Barron J. A., Urbina-Schmitt M., Ochoa D., Esperante R. & Snee L. W. 2021. — The Miocene stratigraphy of the Laberinto area (Río Ica Valley) and its bearing on the geological history of the East Pisco Basin (south-central Peru). *Journal of South American Earth Sciences* 111: 103458. https://doi.org/10.1016/j.jsames.2021.103458

Di Celma C., Malinverno E., Collareta A., Bosio G., Gariboldi K., Lambert O., Landini W., Pierantoni P. P., Gioncada A. & Villa I. 2018. — Facies analysis, stratigraphy and marine vertebrate assemblage of the lower Miocene Chilcatay Formation at Ullujaya (Pisco basin, Peru). *Journal of Maps* 14 (2): 257-268. https://doi.org/10.1080/17445647.2018.1456490

Di Celma C., Pierantoni P. P., Malinverno E., Collareta A., Lambert O., Landini W., Bosio G., Gariboldi K., Gioncada A., Muizon C. de, Molli G., Marx F. G., Varas-Malca R. M., Urbina M. & Bianucci G. 2019. — Allostratigraphy and paleontology of the lower Miocene Chilcatay Formation in the Zamaca area, East Pisco basin, southern Peru. *Journal of Maps* 15 (2): 393-405. https://doi.org/10.1080/17445647.2019.1604439

Flower W. H. 1867. — On the osteology of the cachalot or sperm-whale (*Physeter macrocephalus*). *Transactions of the Zoological Society of London* 6: 309-372. https://doi.org/10.1111/j.1096-3642.1868.tb00580.x

Hocking D. P., Marx F. G., Park T., Fitzgerald E. M. G. & Evans A. R. 2017. — A behavioural framework for the evolution of feeding in predatory aquatic mammals. *Proceedings of the Royal Society B: Biological Sciences* 284 (1850): 20162750. https://doi.org/10.1098/rspb.2016.2750

Kellogg R. 1927. — Study of the skull of a fossil sperm-whale from the Temblor Miocene of southern California. *Publications of the Carnegie Institution of Washington* 346: 1-23.

Kellogg R. 1959. — Description of the skull of *Pomatodelphis inaequalis* Allen. *Bulletin of the Museum of Comparative Zoology* 121: 3-26. https://www.biodiversitylibrary.org/page/4778126

Kellogg R. 1965. — Fossil marine mammals from the Miocene Calvert Formation of Maryland and Virginia. The Miocene Calvert sperm whale *Orycterocetus*. *Bulletin of the United States National Museum* 247 (2): 47-63. https://repository.si.edu/handle/10088/30450

Kiel S., Jakubowicz M., Altamirano A., Belka Z., Dopieralska J., Urbina M. & Salas-Gismondi R. 2023. — The late Cenozoic evolution of the Humboldt Current System in coastal Peru: insights from neodymium isotopes. *Gondwana Research* 116: 104-112. https://doi.org/10.1016/j.gr.2022.12.008

Kimura T. & Hasegawa Y. 2019. — A new species of *Kentriodon* (Cetacea, Odontoceti, Kentriodontidae) from the Miocene of Japan. *Journal of Vertebrate Paleontology*: e1566739. https://doi.org/10.1080/02724634.2019.1566739

Kimura T. & Hasegawa Y. 2022. — A new physeteroid from the lower Miocene of Japan. *Paleontological Research* 26 (1): 87-101. https://doi.org/10.2517/PR200021

Kimura T. & Hasegawa Y. 2023. — Additional rostrum fragments of the holotype of *Miophyseter chitaensis* (in Japanese with English abstract). *Bulletin of the Gunma Museum of Natural History* 27: 107-112.

Lambert O. 2006. — First record of a platanistid (Cetacea, Odontoceti) in the North Sea Basin: a review of *Cyrtodelphis* Abel, 1899 from the Miocene of Belgium. *Oryctos* 6: 69-79.

Lambert O. 2008. — Sperm whales from the Miocene of the North Sea: a re-appraisal. *Bulletin de l'Institut royal des Sciences naturelles de Belgique, Sciences de la Terre* 78: 277-316.

Lambert O. & Bianucci G. 2019. — How to break a sperm whale's teeth: dental damage in a large Miocene physeteroid from the North Sea basin. *Journal of Vertebrate Paleontology*: e1660987. https://doi.org/10.1080/02724634.2019.1660987

Lambert O., Bianucci G. & Urbina M. 2014. — *Huaridelphis raimondii*, a new early Miocene Squalodelphinidae (Cetacea, Odontoceti) from the Chilcatay Formation, Peru. *Journal of Vertebrate Paleontology* 34 (5): 987-1004. https://doi.org/10.1080/02724634.2014.858050

Lambert O., Muizon C., De & Bianucci G. 2015. — A new archaic homodont toothed whale (Mammalia, Cetacea, Odontoceti) from the early Miocene of Peru. *Geodiversitas* 37 (1): 79-108. https://doi.org/10.5252/g2015n1a4

Lambert O., Bianucci G. & Muizon C. de 2017. — Macroraptorial sperm whales (Cetacea, Odontoceti, Physeteroidea) from the Miocene of Peru. *Zoological Journal of the Linnean Society* 179 (2): 404-474. https://doi.org/10.1111/zoj.12456

Lambert O., Muizon C. de, Malinverno E., Di Celma C., Urbina M. & Bianucci G. 2018. — A new odontocete (toothed cetacean) from the Early Miocene of Peru expands the morphological disparity of extinct heterodont dolphins. *Journal of Systematic Palaeontology* 16 (12): 981-1016. https://doi.org/10.1080/14772019.2017.1359689

Lambert O., Muizon C. de, Urbina M. & Bianucci G. 2020. — A new longirostrine sperm whale (Cetacea, Physeteroidea) from the lower Miocene of the Pisco Basin (southern coast of Peru). *Journal of Systematic Palaeontology* 18 (20): 1707-1742. https://doi.org/10.1080/14772019.2020.1805520

Lambert O., Muizon C. de, Varas-Malca R. M., Urbina M. & Bianucci G. 2021. — Eurhinodelphinids from the early Miocene of Peru: first unambiguous records of these hyperlongirostrine dolphins outside the North Atlantic realm. *Rivista Italiana di Paleontologia e Stratigrafia* 127 (1): 17-32. https://doi.org/10.13130/2039-4942/15124

Landini W., Collareta A., Di Celma C., Malinverno E., Urbina M. & Bianucci G. 2019. — The early Miocene elasmobranch assemblage from Zamaca (Chilcatay Formation, Peru). *Journal of South American Earth Sciences* 91: 352-371. https://doi.org/10.1016/j.jsames.2018.08.004

Lavery T. J., Roudnew B., Gill P., Seymour J., Seuront L., Johnson G., Mitchell J. G. & Smetacek V. 2010. — Iron defecation by sperm whales stimulates carbon export in the Southern Ocean. *Proceedings of the Royal Society B: Biological Sciences* 277 (1699): 3527-3531. https://doi.org/10.1098/rspb.2010.0863

Lydekker R. 1893. — Contribution to the knowledge of the fossil vertebrates of Argentina. Part II. Cetacean skulls from Patagonia. *Anales del Museo de La Plata* 1893: 1-14.

Marino L., Sudheimer K., Pabst D. A., Mclellan W. A. & Johnson J. I. 2003. — Magnetic resonance images of the brain of a dwarf sperm whale (*Kogia simus*). *Journal of Anatomy* 203 (1): 57-76. https://doi.org/10.1046/j.1469-7580.2003.00199.x

Marx F. G., Lambert O. & Uhen M. D. 2016. — *Cetacean paleobiology*. John Wiley & Sons, Chichester, UK, Topics in Paleobiology, 319 p. https://doi.org/10.1002/9781118561546

Marx F. G., Fitzgerald E. M. G. & Fordyce R. E. 2019. — Like phoenix from the ashes: How modern baleen whales arose from a fossil "dark age". *Acta Palaeontologica Polonica* 64 (2): 231-238. https://doi.org/10.4202/app.00575.2018

McCurry M. R. & Pyenson N. D. 2019. — Hyper-longirostry and kinematic disparity in extinct toothed whales. *Paleobiology* 45 (1): 21-29. https://doi.org/10.1017/pab.2018.33

Mead J. G. & Fordyce R. E. 2009. — The therian skull: a lexicon with emphasis on the odontocetes. *Smithsonian Contributions to Zoology* 627: 1-248. https://doi.org/10.5479/si.00810282.627

Nelson M. D. & Uhen M. D. 2018. — First occurrence of a squalodelphinid (Cetacea, Odontoceti) from the early Miocene of Washington State. *Journal of Vertebrate Paleontology*: e1428197. https://doi.org/10.1080/02724634.2017.1428197.

Ochoa D., Salas-Gismondi R., DeVries T. J., Baby P., Muizon C. de, Altamirano A., Barbosa-Espitia A., Foster D. A., Quispe K. & Cardich J. 2021. — Late Neogene evolution of the Peruvian margin and its ecosystems: a synthesis from the Sacaco record. *International Journal of Earth Sciences* 110: 995-1025. https://doi.org/10.1007/s00531-021-02003-1

PAOLUCCI F., BUONO M. R., FERNÁNDEZ M. S., MARX F. G. & CUITIÑO J. I. 2020. — *Diaphorocetus poucheti* (Cetacea, Odontoceti, Physeteroidea) from Patagonia, Argentina: one of the earliest sperm whales. *Journal of Systematic Palaeontology* 18 (4): 335-355. https://doi.org/10.1080/14772019.2019.1605544

PAOLUCCI F., FERNÁNDEZ M. S., BUONO M. R. & CUITIÑO J. I. 2021. — '*Aulophyseter*' *rionegrensis* (Cetacea: Odontoceti: Physeteroidea) from the Miocene of Patagonia (Argentina): a reappraisal. *Zoological Journal of the Linnean Society* 192 (4): 1293-1322. https://doi.org/10.1093/zoolinnean/zlaa137

PARRAS A. & CUITIÑO J. I. 2021. — Revised chrono and lithostratigraphy for the Oligocene-Miocene Patagoniense marine deposits in Patagonia: implications for stratigraphic cycles, paleogeography, and major drivers. *Journal of South American Earth Sciences* 110: 103327. https://doi.org/10.1016/j.jsames.2021.103327

PEREDO C. M., UHEN M. D. & NELSON M. D. 2018. — A new kentriodontid (Cetacea: Odontoceti) from the early Miocene Astoria Formation and a revision of the stem delphinidan family Kentriodontidae. *Journal of Vertebrate Paleontology*: e1411357. https://doi.org/10.1080/02724634.2017.1411357

PERI E., COLLARETA A., INSACCO G. & BIANUCCI G. 2019. — An *Inticetus*-like (Cetacea: Odontoceti) postcanine tooth from the Pietra leccese (Miocene, southeastern Italy) and its palaeobiogeographical implications. *Neues Jahrbuch für Geologie und Paläontologie-Abhandlungen* 291 (2): 221-228. https://doi.org/10.1127/njgpa/2019/0799

PERI E., FALKINGHAM P. L., COLLARETA A. & BIANUCCI G. 2022a. — Biting in the Miocene seas: estimation of the bite force of the macroraptorial sperm whale *Zygophyseter varolai* using finite element analysis. *Historical Biology* 34 (10): 1-12. https://doi.org/10.1080/08912963.2021.1986814

PERI E., COLLARETA A., ARINGHIERI G., CARAMELLA D., FORESI L. M. & BIANUCCI G. 2022b. — A new physeteroid cetacean from the Lower Miocene of southern Italy: CT imaging, retrodeformation, systematics and palaeobiology of a sperm whale from the Pietra leccese. *Bollettino della Società Paleontologica Italiana* 61 (2): 187-206. https://doi.org/10.4435/BSPI.2022.15

PYENSON N. D. & SPONBERG S. N. 2011. — Reconstructing body size in extinct crown Cetacea (Neoceti) using allometry, phylogenetic methods and tests from the fossil record. *Journal of Mammalian Evolution* 18 (4): 269-288. https://doi.org/10.1007/s10914-011-9170-1

REICHLER V. A. 2010. — Estratigrafía y paleontología del Cenozoico marino del Gran Bajo y Salinas del Gualicho, Argentina y descripción de 17 especies nuevas. *Andean Geology* 37 (1): 177-219. https://doi.org/10.5027/andgeoV37n1-a08

RICE D. W. 1989. — Sperm whale *Physeter macrocephalus* Linnaeus, 1758, *in* RIDGWAY S. H. & HARRISON R. (eds), *Handbook of Marine Mammals. Vol. 4: River Dolphins and the Larger Toothed Whales*. Academic Press, London: 177-233.

RIES F. A. & LANGWORTHY O. R. 1937. — A study of the surface structure of the brain of the whale (*Balaenoptera physalus* and *Physeter catodon*). *Journal of Comparative Neurology* 68 (1): 1-47. https://doi.org/10.1002/cne.900680102

SHIMADA K., CHANDLER R. E., LAM O. L. T., TANAKA T. & WARD D. J. 2017. — A new elusive otodontid shark (Lamniformes: Otodontidae) from the lower Miocene, and comments on the taxonomy of otodontid genera, including the 'megatoothed' clade. *Historical Biology* 29 (5): 704-714. https://doi.org/10.1080/08912963.2016.1236795

STEEMAN M. E., HEBSGAARD M. B., FORDYCE R. E., HO S. Y. W., RABOSKY D. L., NIELSEN R., RAHBEK C., GLENNER H., SØRENSEN M. V. & WILLERSLEV E. 2009. — Radiation of extant cetaceans driven by restructuring of the oceans. *Systematic Biology* 58 (6): 573-585. https://doi.org/10.1093/sysbio/syp060

SWOFFORD D. L. 2003. — *PAUP*. Phylogenetic analysis using parsimony (*and other methods). Version 4*. Sinauer Associates, Sunderland, Massachusetts.

VELEZ-JUARBE J., WOOD A. R., DE GRACIA C. & HENDY A. J. W. 2015. — Evolutionary patterns among living and fossil kogiid sperm whales: Evidence from the Neogene of Central America. *PLoS ONE* 10 (4): e0123909. https://doi.org/10.1371/journal.pone.0123909

VIGLINO M., BUONO M. R., FORDYCE R. E., CUITIÑO J. I. & FITZGERALD E. M. G. 2019. — Anatomy and phylogeny of the large shark-toothed dolphin *Phoberodon arctirostris* Cabrera, 1926 (Cetacea: Odontoceti) from the early Miocene of Patagonia (Argentina). *Zoological Journal of the Linnean Society* 185 (2): 511-542. https://doi.org/10.1093/zoolinnean/zly053

VIGLINO M., GAETÁN C. M., CUITIÑO J. I. & BUONO M. R. 2021. — First toothless platanistoid from the Early Miocene of Patagonia: the golden age of diversification of the Odontoceti. *Journal of Mammalian Evolution* 28: 337-358. https://doi.org/10.1007/s10914-020-09505-w

VIGLINO M., BUONO M. R., TANAKA Y., CUITIÑO J. I. & FORDYCE R. E. 2022. — Unravelling the identity of the platanistoid *Notocetus vanbenedeni* Moreno, 1892 (Cetacea, Odontoceti) from the early Miocene of Patagonia (Argentina). *Journal of Systematic Palaeontology* 20 (1): 2082890. https://doi.org/10.1080/14772019.2022.2082890

WERTH A. J. 2004. — Functional morphology of the sperm whale tongue, with reference to suction feeding. *Aquatic Mammals* 30: 405-418. https://doi.org/10.1578/AM.30.3.2004.405

Submitted on 5 April 2023
accepted on 18 July 2023
published on 30 November 2023.

APPENDIX 1. — Textured 3D model of the cranium of *Diaphorocetus ortegai* n. sp. MUSM 3246 (holotype) obtained with an Artec Eva structured-light scanner. https://doi.org/10.5852/geodiversitas2023v45a22_s1

APPENDIX 2. — Textured 3D model of the cranium of *Rhaphicetus valenciae* Lambert, Muizon, Urbina & Bianucci, 2020 MUSM 2543 (holotype) obtained with a SHINING EinScan Pro HD structured-light scanner. The two parts of the cranium (anterior two thirds of rostrum and rest of the skull) were assembled with Blender 3.0.1. https://doi.org/10.5852/geodiversitas2023v45a22_s2

APPENDIX 3. — Textured 3D model of the skull of *Acrophyseter robustus* Lambert, Bianucci & Muizon, 2016 MUSM 1399 (holotype) obtained with a SHINING EinScan Pro HD structured-light scanner. The two parts of the skull (tip of snout and rest of the skull) were assembled with Blender 3.0.1. https://doi.org/10.5852/geodiversitas2023v45a22_s3

APPENDIX 4. — Character-taxon matrix, modified from Peri *et al.* (2022b). Changes in the scores for *Acrophyseter robustus* Lambert, Bianucci & Muizon, 2016 and *Diaphorocetus poucheti* (Moreno, 1892) and scores for four new characters are highlighted in red. https://doi.org/10.5852/geodiversitas2023v45a22_s4

Appendix 5. — Strict consensus of 15 most parsimonious trees resulting from the heuristic search performed with down-weighting of homoplastic characters (k = 3). Tree length 188; Goloboff fit -42.64; CI 0.45; RI 0.68.